

RAI: Volume 3, Chapter 2.2.1.3.4, First Set, Number 2:

Describe the TSPA implementation of colloid formation (e.g., Pu-239) and radionuclide release (e.g., Tc-99) occurring from rapid mobilization (or dissolution) of (i) the commercial SNF and HLW glass under igneous intrusive conditions and (ii) the DOE-owned SNF under nominal and igneous intrusive conditions.

Basis: The applicant presented the bounding assumption in the radionuclide release from the commercial SNF and HLW glass under igneous intrusive conditions in SAR 2.3.11.3.2.4. To avoid underestimating radionuclide mobility, the applicant assumed that all commercial SNF and HLW glass in the drifts is unprotected, instantaneously degraded, and the radionuclides are immediately available for mobilization by groundwater (SNL 2007, Section 8.1). Similarly, the applicant assumed in SAR 2.3.7.8.1 that the DOE-owned SNF degrades instantaneously upon waste package breach (BSC 2004b, Section 6.2 and 8.1). The applicant needs to describe how its bounding assumption addresses (i) colloid formation and precipitation of actinides such as Pu-239, and (ii) faster release of highly soluble radionuclides such as Tc-99 or I-129. The requested information is needed to verify compliance with 10 CFR 63.21(c)(9), (12) and (15) and 63.114(b) and (g).

1. RESPONSE**1.1 WASTE FORM DEGRADATION AND MOBILIZATION FOR THE IGNEOUS INTRUSION MODELING CASE**

The disposition of the radionuclides mobilized in the igneous intrusion modeling case is evaluated using the nominal scenario class total system performance assessment (TSPA) model components and submodels with a few scenario-specific changes. The modifications to the nominal scenario class components and submodels affecting radionuclide mobilization in the igneous intrusion modeling case are as follows (SAR Section 2.4.2.3.2.1.12.2; SNL 2008, Section 6.5.1.1):

- The drip shields and waste packages provide no hindrance to flow after the time of the igneous intrusion event.
- The three modeled waste forms (commercial spent nuclear fuel (SNF), U.S. Department of Energy (DOE) SNF (DOE SNF), and high-level waste (HLW) glass) are assumed to be completely degraded at the time of the igneous intrusion event. The radionuclides in the commercial SNF, DOE SNF, and HLW are considered immediately available for dissolution and transport (SNL 2008, Section 6.5.1).
- All of the intruded drifts (i.e., all waste package locations, including those in a non-seeping environment under nominal conditions) have seepage equal to the local

percolation (SNL 2008, Section 6.5.1). The seepage model is not used after the igneous intrusion event.

- In the igneous intrusion modeling case, all Engineered Barrier System (EBS) and in-package chemistry-related submodels and parameters are the same as in the nominal scenario class modeling case, with the exception of the uranium solubility submodel. As indicated in SAR Section 2.4.2.3.2.1.7, method 2 for uranium solubility is used for the igneous intrusion modeling case. Method 2 is based on the presence of silica in the aqueous environment. In particular, the presence of basalt in the drifts necessitates that Na-boltwoodite needs to be included as a uranium solubility-controlling phase. More specifically, two additional base solubility lookup tables are defined for this case, which include schoepite, Na-boltwoodite, and $\text{Na}_4\text{UO}_2(\text{CO}_3)_3$, depending on the pH and f_{CO_2} .
- The EBS thermal-hydrologic environment submodel for the igneous intrusion modeling case differs from that used for the nominal scenario class modeling case, in that it accounts for the temperature increase within and around the drift due to the intrusion of magma that fills the drift (SAR Section 2.4.2.3.2.1.12.2).

The EBS radionuclide flow and transport model (SAR Section 2.3.7.12) predicts movement of dissolved and colloidal radionuclides through the waste form, out of the waste package, and through the invert. The dissolved radionuclide concentration model determines the solubility of radionuclides for a particular water chemistry (SAR Section 2.3.7.10), and the colloid model determines the mobilization of radionuclides attached to colloids (SAR Section 2.3.7.11). In the nominal modeling case, the amount of dissolved mass of highly soluble radionuclides (e.g., ^{99}Tc and ^{129}I) is dependent on the waste form degradation rates (SAR Section 2.4.2.2.1.1.3), whereas for the igneous intrusion modeling case, the entire mass of these radionuclides are available for transport after the event occurs.

1.1.1 Waste Form Colloid Formation

For all modeling cases, including igneous intrusion, waste form colloids are generated in the waste form domain through degradation of commercial SNF, HLW glass, and DOE SNF; iron oxyhydroxide colloids are generated in the corrosion products domain; and naturally occurring ground water colloids are present in the natural system (SNL 2007a, Section 6.5.2.5). The focus of this RAI response is on the formation of waste form-generated colloids.

Waste form colloids originate by the spallation of radionuclide bearing alteration phases from the waste form that are within colloidal size range and by the nucleation (co-precipitation) of colloids from ions dissolved from the waste form and sorption of ionic radionuclides or radionuclide-bearing phases (SNL 2007b, Section 6.3.1, Figure 6-2). Radionuclides may be attached to waste form colloids in several ways. In some cases the attachment and detachment is relatively fast compared to the residence time (in a given transport domain) and can be described as an equilibrium sorption process and modeled via a K_d value. In other cases attachment may be fast but detachment very slow relative to the residence time (in a given transport domain), as in co-precipitation where the radionuclide becomes embedded in the host colloid. This type of attachment is referred to as irreversible sorption and modeled via kinetic attachment. Sorption of

radionuclides on various types of waste form colloids is modeled as follows (SAR 2.3.7.11.3 and SNL 2008, Section 6.3.7.6.1):

1. HLW glass degradation colloids – reversible and irreversible
2. Commercial SNF degradation rind colloids – irreversible
3. DOE and commercial SNF uranium mineral colloids – reversible.

At each time step executed in the TSPA model calculation, the colloid model evaluates the characteristics of the water in the waste package (ionic strength and pH) to determine the formation of irreversible waste form colloids. At each time step, the ionic strength threshold above which the colloid suspensions are unstable is defined by a simple function of pH of the waste package water. When colloid suspensions are unstable (i.e., ionic strength in the waste package exceeds the threshold value), a low (non-zero) limit of colloid concentration is used (SNL 2007b, Section 6.5). When the ionic strength in the waste packages is below the threshold value for colloid suspension stability, the colloid model is used to calculate the mass concentration of SNF- and HLW-generated waste form colloids and the concentration of plutonium and americium irreversibly attached to (i.e., embedded in) these colloids. The TSPA model calculates the concentrations of the waste form colloid as a function of solution chemistry inside the breached waste package. The TSPA model also calculates the continual interaction of these colloids with radionuclide-bearing fluids and calculates the partitioning of radionuclides onto colloid surfaces (reversibly attached).

1.1.1.1 Generation of Commercial SNF and HLW Glass Irreversible Waste Form Colloids

This section discusses implementation of waste form colloid formation from the commercial SNF and HLW glass waste forms under igneous intrusive conditions. As discussed in Section 6.5.2.5 and defined in Equation 6.5.2.5-12 of *EBS Radionuclide Transport Abstraction* (SNL 2007a), the conversion of plutonium to plutonium embedded in waste form colloids occurs in the waste form domain. The conversion rate is a function of the available plutonium in the waste form domain and predicted colloid concentrations. The predicted colloid concentrations, including the mass of plutonium in the colloid suspension, are determined by the colloid model. For the HLW glass and commercial SNF colloids, the distributions of waste form colloid concentrations (see range for *CPu_Col_WF_EMBED_Sampled_a* and *CPu_Col_CSNF_Sampled_a* in SNL 2008, Tables 6.3.7-62 and 6.3.7-63) are sampled (once per realization) and then the stability of the colloid suspension is tested based on the ionic strength and pH of the water in the waste form domain. The stability of the colloid suspension is determined from the stability field (SNL 2008, Figure 6.3.7-11). If found stable, the sampled value is chosen, otherwise the minimum value (10^{-13} mol/l) (*CPu_Col_Glass_EMBED_Min* and *CPu_Col_CSNF_Min*) is selected. In addition, the concentration range of plutonium associated with a unit colloid concentration is also sampled (see range for *CPu_Per_WF_EMBED_Col_a* and *CPu_Per_CSNF_EMBED_Col_a* in SNL 2008, Tables 6.3.7-62 and 6.3.7-63). The ratio of the concentration of plutonium embedded in a colloid and the aqueous concentration of plutonium

associated within colloid suspensions when colloid suspensions are stable provides the colloid conversion rate. A similar calculation is performed for americium.

Provided that there is available plutonium (C_i) in the waste form domain, the conversion of available plutonium to plutonium embedded in colloids continues at a rate (λ_i^{embed}) that is consistent with Equation 6.5.2.5-12 of *EBS Radionuclide Transport Abstraction* (SNL 2007a) (reproduced here as Equation 1):

$$\lambda_i^{embed} = \frac{\left(\theta_w C_i^{embed} \right)^{n+1} - \left(\theta_w C_i^{embed} \right)^n}{\Delta t} + \left(Q_{adv/diff}^{wfc} \frac{C_i^{embed}}{C_{cWF}} \right)^n \quad (\text{Eq. 1})$$

In this equation the term $(\theta_w C_i^{embed})^{n+1}$ denotes the predicted mass of plutonium that is embedded in colloids associated with stable or unstable suspensions at the n+1 timestep. The term $(\theta_w C_i^{embed})^n$ is calculated as the mass that has already been converted to the embedded colloid phase in the TSPA model. Together these two terms make up the accumulation term in the production rate.

The term $\left(Q_{adv/diff}^{wfc} \frac{C_i^{embed}}{C_{cWF}} \right)^n$ accounts for the removal of the colloid suspension from the waste form domain by advection and/or diffusion. The concentration of plutonium embedded in a colloid (C_i^{embed}) and the aqueous concentration of plutonium associated within colloid suspensions when colloid suspensions are stable (C_{cWF}) are epistemic quantities that are sampled independent of the modeling case performed (SNL 2008, Table 6.3.7-62). As such, the process of irreversible waste form colloid production in the TSPA model continues whether the waste form is fully degraded or not. As long as there is plutonium or americium available in the waste form domain, irreversible waste form colloids are produced in the waste form domain.

In the igneous intrusion modeling case the SNF and the HLW glass degrade instantly. The released mass may dissolve, precipitate, and/or become associated with colloids (sorbed) and colloid suspensions (embedded). The conversion of plutonium and americium to irreversible colloids is modeled as a first order reaction applying a rate constant and evaluating the total mass concentration in the waste form domain (SNL 2007a, p. 6-220). However, the referenced document (SNL 2007a) incorrectly states on page 6-220 and in Equation 6.5.1.2-9 that the dissolved concentration is used to calculate the colloid conversion rates. In the TSPA-LA model, the total concentration in all phases, including any available stationary mass (i.e., precipitated mass) is available for the formation of waste form colloids. Thus, the denominator of Equation 1 is the total concentration in all phases in the TSPA model and the documentation error does not impact the license application technical baseline or the TSPA-LA model results. A revision to the referenced document is currently in process to replace “dissolved concentration” with total

radionuclide mass (total concentration) in the domain. Final resolution of this issue is not expected to require a change to the license application.

In the igneous intrusion modeling case the in-package ionic strength of the waste form domain is determined using the liquid influx submodel, which results in lower ionic strength values for increasing liquid flux (SAR Section 2.3.7.5.3.1). As discussed previously, the application of percolation rates to all waste package locations in the igneous intrusion modeling case increases the flux rates through the waste packages (compared to the nominal modeling case) and, as a result, colloid suspensions are more likely to be stable and the contribution of colloids to radionuclide mobility increases.

In the nominal modeling case the in-package ionic strength is determined using the vapor influx submodel prior to the formation of general corrosion patch openings in the waste package. Because there is a minimum of water to dissolve solids and flush salts out of the cells, the in-package ionic strength determined using the vapor influx model is generally higher than the in-package ionic strength determined using the liquid influx model. Higher ionic strengths may result in unstable colloid suspensions resulting in a decreased production of waste form colloids. Generally, when the liquid influx model is used to calculate the in-package water chemistry, even though colloid suspensions are more likely to be stable in the waste form domain, the water chemistry induces slower waste form degradation rates. Consequently, the availability of americium and plutonium in the waste form domain may be limited, and the conversion from available mass to mass that is embedded within irreversible colloids will be decreased compared to the igneous intrusion modeling case.

1.1.1.2 Generation of Commercial and DOE SNF Uranium Waste Form Colloids

This section discusses the generation of uranium mineral waste form colloids from DOE-owned SNF, instantaneously degraded under nominal and igneous intrusive conditions and commercial SNF, which is also instantaneously degraded in the igneous intrusive case. For DOE SNF, which comprises a small fraction of the repository inventory, the uranium metal fuels alter to hydrated and/or oxidized secondary phases that might ultimately be transported colloidally. Likewise, oxidized uranium phases have been observed in solutions in contact with degrading commercial SNF. The generation of commercial and DOE SNF uranium waste form colloids is evaluated in the igneous intrusion modeling case identically to the nominal modeling case, except, as discussed previously, the application of percolation rates to all waste package locations in the igneous intrusion modeling case increases the flux rates through the waste packages (compared to the nominal modeling case) and, as a result, colloid suspensions are more likely to be stable and the contribution of colloids to radionuclide release increases.

The commercial and DOE SNF waste forms generate uranium mineral colloids that are conceptually identified as uranophane and modeled as meta-autunite with reversibly sorbed plutonium, thorium, protactinium, americium, neptunium, cesium, radium, and tin (SAR Section 2.3.7.11.1). Only reversible sorption onto these colloids is modeled using K_d values that describe the distribution of radionuclides between the fluid and the uranium(VI) phase (uranophane) colloids. Calculation of the predicted concentrations of reversible SNF (uranophane) colloids is done similarly to the method used for the generation of waste form

colloids. A cumulative distribution from 0.001 to 200 mg/L is sampled once per realization to establish the concentration of reversible SNF (uranophane) colloids within the waste form (SAR Section 2.3.7.113). Then, at each TSPA-LA model time step, the waste package water chemistry is evaluated to determine the meta-autunite stability for DOE SNF and commercial SNF uranophane colloids as per the following relationship between pH and ionic strength; $I_{threshold} = (0.008 \times pH^2) \cdot (0.14 \times pH) - 0.4$ (SAR Figure 2.3.7-44). If the colloid suspension is deemed unstable, the colloid concentration is set to a very low nonzero value, which is typically 10^{-6} mg/l (SAR Section 2.3.7.113). The mass of radionuclides reversibly sorbed onto SNF colloids is calculated from the sampled mass concentration of uranophane colloids, K_d values describing the distribution of radionuclides (plutonium, neptunium, americium, thorium, protactinium, radium, cesium, and tin) between the fluid and uranophane colloids, and the dissolved concentration of radionuclides as calculated in the EBS transport model for the TSPA (SNL 2007a, Section 6.5.2.5, Equation 6.5.2.5-1). The sorption capacity model described in Section 6.3.12.3 of *Waste Form and In-Drift Colloids-Associated Radionuclide Concentrations: Abstraction and Summary* (SNL 2007b), is used to partition the sorption of different radionuclide species onto the uranophane colloids in proportion to their sampled K_d values.

The DOE SNF waste form is in codisposal waste packages. The DOE SNF waste form colloids are calculated within the codisposal waste package domain for waste form Cell 1b (DOE SNF waste form subdomain) in the TSPA model (SNL 2008, Section 6.3.8.3). In all modeling cases, including the igneous intrusion modeling case, the DOE SNF waste form instantly degrades upon waste package breach and the inventory is released to the DOE SNF waste form subdomain. The released mass may dissolve, precipitate, and/or become associated with colloids. When the DOE SNF waste form is instantly degraded, the mass in the waste form domain increases, which supports the maximum calculated uranophane colloid conversion rates.

1.1.2 Radionuclide Mobilization

This section describes the TSPA implementation of mobile radionuclide releases (e.g., ^{99}Tc) occurring from degradation of the commercial SNF and HLW glass and the DOE SNF under nominal and igneous intrusive conditions. The waste form degradation and mobilization model component simulates the degradation of commercial SNF, DOE SNF, and HLW glass waste and the subsequent dissolution of their radionuclide inventories into the liquid phase present in the degraded waste. SAR Section 2.3.7 describes this mobilization of radionuclide mass as either dissolved species or as attached to colloidal particles. The waste form degradation and mobilization model component accounts for in-package water chemistry; matrix degradation rates for commercial SNF, DOE SNF, and HLW glass waste forms; radionuclide solubilities; and the types and concentrations of waste-form, groundwater, and iron oxyhydroxide colloids.

SAR Section 2.3.7 also describes the EBS flow and transport model component, which calculates the rate of radionuclide release from the EBS to the unsaturated zone. This component simulates the rate of water flow through the EBS, diffusive and advective transport of dissolved radionuclides, sorption, and colloid-facilitated transport.

The one-dimensional mass balance equation describing transport of dissolved and reversibly sorbed radionuclide species is provided in Equation 6.5.1.2-47 of *EBS Radionuclide Transport*

Abstraction (SNL 2007a). Within the waste form domain there are no groundwater or iron oxyhydroxide colloids and no immobile corrosion product material, which simplifies the one-dimensional transport equation, (SNL 2007a, Eq. 6.5.1.2-47), because the terms associated with these processes will be zero (SNL 2007a, Section 6.5.1.2, p. 6-160). The initial concentration for all radionuclides is zero. The upstream boundary to the waste form domain maintains a zero radionuclide flux condition. Radionuclide concentrations will remain zero until waste package failure.

At the time of waste package failure the waste form is exposed and DOE SNF is instantly degraded in all modeling cases, while commercial SNF and HLW glass are also instantly degraded in the igneous intrusion modeling case. The radionuclides released into the waste form domain (Cell 1a for commercial SNF and HLW and Cell 1b for DOE SNF) are partitioned between dissolved, irreversibly sorbed on colloids, reversibly sorbed on colloids, and precipitated mass (SNL 2008, Section 6.3.8.2). Partitioning of the mass between these processes is dependent upon the in-package water chemistry, available mass, dissolved concentration limits, colloid stability, embedded colloid conversion rates (described previously), and sorption onto waste form colloids. The dissolved concentration component of the transport equation is limited by the radionuclide dissolved concentration limit. Colloid mobilization is limited only by the stability of colloid suspensions defined within the waste form domain, the calculated conversion rates for mass that is irreversibly attached to waste form colloids, and partition coefficient for mass that is reversibly sorbed onto waste form colloids.

For highly mobile radionuclides (e.g., ^{99}Tc), the entire mass is assumed to be dissolved and available for transport via both advection and diffusion processes (SNL 2008, Section 6.3.7.5.2). These processes are identical for commercial SNF, DOE SNF and HLW waste form domains, except as noted for colloid formation. Dissolved species are transported by advection and diffusion downstream to the corrosion products domain. The upstream boundary condition for the corrosion products domain is controlled by the flux out of the waste form domain. From the corrosion products domain, the mobile radionuclides will migrate through the invert and then into the unsaturated zone.

As discussed earlier in this RAI response, the disposition of the radionuclides mobilized by the igneous intrusion is generally evaluated using the nominal scenario class TSPA model components and submodels for flow and transport of the released radionuclides in the waste package and invert of the EBS, unsaturated zone, and saturated zone. Specific differences for the igneous intrusion modeling case include the transport of radionuclides out of the EBS primarily by advection, because the drip shield has been compromised and the waste package has lost its integrity to flow, and water contacting the waste is equal to the local percolation traveling through the host rock (SNL 2008, Section 6.5.1.1). In addition, as indicated in SAR Section 2.4.2.3.2.1.7, method 2 for uranium solubility is used as well as adjustments to the in-package chemistry and temperature increase within and around the drift due to the intrusion of magma that fills the drift in the igneous intrusion modeling case. The waste-package inner vessels and outer barriers, and the waste forms (commercial SNF, HLW, and DOE SNF) are considered fully degraded at the time of the event. Both the geometry of the waste form (which is important for diffusive transport) and the formation of corrosion products from degradation of the waste package are assumed to be the same as in the nominal scenario class. In the nominal

modeling case advection only occurs in the dripping environments after the drip shield has failed over a breached waste package and water flows into a breached waste package as described by the seepage model.

The bounding assumption of instantaneous degradation of DOE SNF in all modeling cases and commercial SNF and HLW glass in the igneous intrusion modeling case causes all highly mobile species (e.g., ^{99}Tc) to be available for immediate mobilization and transport. This a conservative assumption because immediate mobilization of non-sorbing radionuclide mass can generally result in higher peak EBS release rates for these species.

1.2 SUMMARY

The disposition of the radionuclides mobilized in the igneous intrusion modeling case is evaluated using the nominal scenario class TSPA model components and submodels with a few scenario-specific changes. The modifications to the nominal scenario class components and submodels affecting radionuclide mobilization in the igneous intrusion modeling case have been described in this response and are detailed in SAR Section 2.4.2.3.2.1.12.2 and in Section 6.5.1.1 of *Total System Performance Assessment Model /Analysis for the License Application* (SNL 2008). For all modeling cases, including igneous intrusion, waste form colloids are generated in the waste form domain through degradation of commercial SNF, HLW glass, and DOE SNF and the colloid generation is a function of the available mass (e.g., plutonium) in the waste form domain and the predicted colloid conversion rate. This response describes the release of mobile radionuclides (e.g., ^{99}Tc) occurring from instant degradation of the commercial SNF and HLW glass and the DOE-owned SNF after an igneous intrusion event. In the igneous intrusion modeling case (and all modeling cases for DOE-owned SNF) all highly mobile species (e.g., ^{99}Tc) are available for immediate mobilization and transport. This a conservative assumption because immediate mobilization of non-sorbing radionuclide mass will generally result in higher peak EBS release rates for those species.

2. COMMITMENTS TO NRC

None.

3. DESCRIPTION OF PROPOSED LA CHANGE

None.

4. REFERENCES

SNL (Sandia National Laboratories) 2007a. *EBS Radionuclide Transport Abstraction*. ANL-WIS-PA-000001 REV 03. Las Vegas, Nevada: Sandia National Laboratories.
ACC: DOC.20071004.0001.

SNL 2007b. *Waste Form and In-Drift Colloids-Associated Radionuclide Concentrations: Abstraction and Summary*. MDL-EBS-PA-000004 REV 03. Las Vegas, Nevada: Sandia National Laboratories. ACC: DOC.20071018.0019; LLR.20080325.0281.^a

ENCLOSURE 1

Response Tracking Number: 00251-00-00

RAI: 3.2.2.1.3.4-002

SNL 2008. *Total System Performance Assessment Model /Analysis for the License Application.* MDL-WIS-PA-000005 REV 00 AD 01. Las Vegas, Nevada: Sandia National Laboratories. ACC: DOC.20080312.0001; LLR.20080414.0037; LLR.20080507.0002; LLR.20080522.0113; DOC.20080724.0005; DOC.20090106.0001.

NOTE: ^aProvided as an enclosure to letter from Williams to Sulima dtd 02/17/2009. "Yucca Mountain – Request for Additional Information Re: License Application (Safety Analysis Report Section 2.1), Safety Evaluation Report Volume 3 – Postclosure Chapters 2.2.1.1 and 2.2.1.3.7 – Submittal of Department of Energy Reference Citations"

RAI: Volume 3, Chapter 2.2.1.3.4, First Set, Number 3:

Justify the assumption that crack surface areas for HLW glass in the seismic scenario and under conditions of glass alteration are the same as those for the nominal case scenarios.

Also, provide bases for the assumption that only half of the cracked surfaces would be exposed to water vapor during dissolution in the vapor-phase aqueous environment.

Basis: The exposed surface area of the glass is important in assessing the radionuclide release from the glass dissolution. The applicant modeled surface area increase from cracking during vitrification in SAR 2.3.7.9.3 (and BSC 2004c, Section 6.6, Table 6-14). The exposure (i.e., increase) factor was represented by a triangular distribution with values from 4 to 17 (maximum probability at 4) in the nominal case (Table 2.4-11, SAR 2.4-400). The applicant estimated this distribution from the thermal cracking during the vitrification, the probability-weighted cracking from inadvertent handling, and the accessibility of water to tight cracks. However, the applicant did not provide the exposure factor under seismic conditions. Under seismic conditions there could be additional cracking. Under both nominal and seismic conditions, the applicant did not consider additional cracking due to potential volume increase of glass alteration products. The intact portion of glass may be subject to stress induced by the expansion of the alteration products during the glass dissolution (Abrajano, et al, 1990).

The bases for DOE's assumption that only half of the cracked surface would be exposed to vapor phase for inducing hydration and subsequent radionuclide release is unclear. Exposure to more than half the cracked surface area would seem to increase release rates; therefore, this assumption seems to be potentially non-conservative. It is also unclear whether more surface area releases both high solubility radionuclides (e.g., dissolved Tc-99) and low solubility radionuclides (e.g., Pu-239 colloids). The requested information is needed to verify compliance with 10 CFR 63.21(c)(9), (12) and (15) and 63.114(b) and (g).

1. RESPONSE

The probability-weighted effects of seismic cracking on the exposure factor uncertainty distribution are negligible. The approach involves considering the effects of seismic-induced impacts (between the codisposal packages and other packages, between the codisposal packages and their support pallets, and between the codisposal packages and the drip shield) (SNL 2007, Sections 6.4.6 and 6.4.7). The effects of these events on glass cracking are addressed by considering the bounding (most severe) event probabilities and comparing the range of seismic impact velocities for these bounding events to the velocities of drop impacts that were used in establishing the crack surface areas for the nominal case (Smith and Ross 1975, Figure 41). *Impact Testing of Vitreous Simulated High-Level Waste in Canisters* (Smith and Ross 1975,

Figure 41) provides experimental data showing the fractional increase in surface area as a function of impact velocity with an unyielding surface. These data show that the fractional increase in surface area is likely to be negligible for impacts associated with the more probable seismic events and small for the less probable and more severe seismic events.

The response builds on the justification provided in *Defense HLW Glass Degradation Model* (BSC 2004, Assumption 5.1), to “establish that the exposed surface area contacted by water is less than the calculated surface area, including the contribution of cracks.” This response justifies the assumption that only half of the cracked surfaces are exposed in estimating the lower end of the uncertainty distribution range of the “exposure factor.” It does so by discussing pertinent experimental data on the corrosion of glass with simulated and actual fracture surfaces.

The response also addresses the potential effects of volume expansion of glass corrosion products on glass cracking by discussing pertinent experimental data to show that this hypothetical process is not expected.

1.1 GLASS CRACKING EXPOSURE FACTOR UNCERTAINTY DISTRIBUTION FOR SEISMIC CASES

Seismic-induced impacts of Engineered Barrier System (EBS) components can occur due to asynchronous movement of the EBS components in response to vibratory ground movement (SNL 2007). Impact velocities (between waste packages, between codisposal packages and their support pallets, and between codisposal packages and the drip shield) are available based on analysis of the kinematic response of the EBS components to seismic events (SNL 2007, Section 6.3). Separate kinematic calculations were performed for 17 ground motion time histories for each of four seismic peak ground velocity (PGV) levels. The four PGV levels and their annual exceedance probabilities are: 10^{-4} per year for PGV level of 0.4019 m/s, 10^{-5} per year for PGV level of 1.05 m/s, 4.5×10^{-7} per year for PGV level of 2.44 m/s, and 10^{-8} per year for PGV level of 4.07 m/s (SNL 2007, Section 6.1, p. 6-2), as shown in Table 1. Because the range of the waste package to waste package impact velocities is similar to the range of the impact velocities with the other EBS components (SNL 2007, Section 6.3), and because the effects of all of the impacts on glass cracking are treated as if they were impacts with an unyielding surface, the following discussion is limited to impacts of the codisposal packages with other waste packages because of the large masses involved. The maximum impact velocities calculated for each of the 17 time histories associated with each of these four PGV levels are summarized in *Mechanical Assessment of Degraded Waste Packages and Drip Shields Subject to Vibratory Ground Motion* (SNL 2007, Table F-5). Only one of the 17 time histories produced an impact (impact velocity of 0.394 m/s or 1.293 fps) at the 0.4019 m/s PGV level. For the other three PGV levels, most of the 17 time histories caused impacts. The average and maximum impact velocities for 17 ground motion time histories at each PGV level, as shown in Table 1, are used to assess the effects of seismic impacts on glass cracking.

Table 1. Impact Velocities Between a Codisposal Waste Package and a TAD-Bearing Waste Package

| Annual Exceedance Probability | PGV (m/s) | Average Impact Velocity (m/s) | Average Impact Velocity (ft/s) | Maximum Impact Velocity (m/s) | Maximum Impact Velocity (ft/s) |
|-------------------------------|-----------|-------------------------------|--------------------------------|-------------------------------|--------------------------------|
| 10^{-4} | 0.40 | .0394 | 1.293 | 0.394 | 1.293 |
| 10^{-5} | 1.05 | 0.755 | 2.476 | 2.148 | 7.047 |
| 10^{-7} | 2.44 | 1.884 | 6.180 | 4.165 | 13.665 |
| 10^{-8} | 4.07 | 3.485 | 11.433 | 9.637 | 31.617 |

Source of data that are averaged in this table: SNL 2007, Table F-5.

NOTE: TAD = transportation, aging, and disposal (canister).

Available testing results (Smith and Ross 1975) correlate the extent of glass cracking (specifically, the fractional increase in geometric area) due to impact with an unyielding surface to the impact velocity (Smith and Ross 1975, Figure 41). These test data show that the best estimate increase in surface area associated with glass cracking due to an impact velocity corresponding to the maximum value of about 32 fps (the maximum impact velocity value calculated at the 4.07 m/s PGV level) is expected to cause a fractional increase in surface area of about 120% (estimated from Smith and Ross 1975, Figure 41). Because such a bounding case is realized in only one of the 17 ground motion time histories at the 4.07 m/s PGV level (which has an annual exceedance probability of 10^{-8}), this surface area increase is unlikely. The average of the maximum impact velocities for the 4.07 m/s PGV level (i.e., 11.433 fps) is expected to produce a fractional increase of about 15% (estimated from Smith and Ross 1975, Figure 41). This same figure shows that the fractional increase in surface area is about 25% for the bounding estimate of the maximum impact velocities (13.665 fps) at the 2.44 m/s PGV level (which has an annual exceedance probability of 4.5×10^{-7}). Even for the more severe low probability seismic events, the expected glass cracking impacts are small; the impacts associated with the more probable seismic events that produce PGV values less than the 2.44 m/s PGV level cause correspondingly smaller fractional increases in the glass surface area. A 25% increase in the extent of cracking is small compared to the extent of cracking associated with cooling and handling, and therefore does not contribute significantly to the uncertainty distribution for the $f_{exposure}$ parameter. The more probable seismic events will cause impact velocities that are expected to be sufficiently low to result in a negligible increase in the extent of glass cracking. Therefore, the probability-weighted effects of seismic cracking on the glass exposure factor uncertainty distribution are expected to be negligible.

1.2 BASIS FOR ASSUMPTION OF EXPOSURE OF HALF OF CRACKED SURFACES

As described in *Defense HLW Glass Degradation Model* (BSC 2004, Section 5.1), and as implemented in calculating the range of the uncertainty distribution for the “exposure factor” ($f_{exposure}$) (BSC 2004, Section 6.5.4) for glass fracture surfaces, the high end of the range is based on assuming free access of water to all of the cracked surfaces and the low end of the range assumes that “50% of the crack surfaces are contacted by water and have a reaction rate that is 50% of the rate at the free surface of the glass.”

Available data show that glass corrosion and leaching at fracture surfaces inside cracks is lower than the corresponding rates at exposed external surfaces (BSC 2004, Section 6.5.4) and has led to the conclusion that “the assumption that crack surfaces leach as readily as external surfaces is unduly conservative” (BSC 2004, Section 6.5.4). Experimental studies using different simulated crack widths showed that the extent to which the leaching at crack surfaces is reduced compared to the exposed external surfaces depends on the crack width (Perez and Westsik 1981). No leaching was observed from tight cracks, and the leaching from cracks with small openings was found to be less than the leaching from exposed surfaces (Perez and Westsik 1981). Results from larger-scale leaching tests conducted on as-cut samples from a 24-inch diameter canister containing thermally cracked glass showed that the leaching rate was within a factor of three times the rates measured on small size samples with a polished (600-grit) finish when only the area of the cut surfaces was used to calculate the leaching rate of the large-scale samples (Bickford and Pellarin 1987). The less than a factor of three increase observed in the leaching of these large-scale thermally cracked samples was attributed mostly to roughness of the cut surfaces, despite the fact that the samples included fracture surface areas estimated to be from 25 to 35 times the surface area of the unfractured monolith. This indicates that the fracture surfaces contributed little to the observed leaching rate.

The experimental observations described above can be attributed to limitations that the fracture openings impose on the rate of transport of water to support the hydrolysis reactions that corrode the glass at the fracture surfaces (i.e., to the fracture surface “accessibility” factor), or to the limitations imposed on the dissolution rate of the glass due to rapid silica saturation of the small volumes of water available inside the fractures (i.e., to the surface “reactivity” factor). Both factors are uncertain. The possible range of both factors for cracked surfaces is 0 to 1. The experimental results cited above indicate that the lower end of the range is close to 0 for very tight cracks but is somewhat larger for wider cracks. Because of uncertainty in the fracture widths in the glass logs and because the future evolution of the fracture widths is also uncertain, it is reasonable to use the value of 1 for both the “accessibility” and “exposure” factors in setting the upper end of the $f_{exposure}$ factor range (BSC 2004, p. 6-45). The assumption that the value is 0.5 (i.e., the midpoint of the possible range) for the “accessibility” and “exposure” factors in evaluating the lower end of the $f_{exposure}$ factor range (BSC 2004, p. 6-45) is reasonable given that the available data indicate that 0.5 probably conservatively overestimates the actual value.

1.3 EFFECTS OF GLASS ALTERATION PRODUCTS ON CRACKING

Corrosion products produced during glass corrosion exhibit a complex composition and structure/microstructure that varies with time (e.g., Abrajano et al. 1990; Crovisier et al. 1986). The estimated bulk density of the alteration products observed under vapor hydration test conditions indicate that the density of the alteration layers can be considerably less than (approximately half) the density of the corroding glass (Jiricka et al. 2001). This indicates that volume expansion associated with formation of alteration products in cracks could potentially cause additional glass fracturing. However, studies of the dissolution of basaltic glass in seawater indicate that volume conservation can occur during the corrosion process (Crovisier et al. 1986, p. 2988). Laboratory tests of cracked glass do not report evidence of cracking due to volume expansion of the glass corrosion products (note that, because glass is brittle, any crack deformation caused by the volume expansion of corrosion products should be observed quickly

in the reaction progress). To the contrary, available evidence (e.g., Pederson et al. 1983, Figure 6) indicates that volume expansion associated with corrosion of glass at the location of a crack did not cause propagation of the fracture. Instead, Pederson et al. (1983, Figure 6) show that the corrosion of the glass at the location of the crack produced a rounded pit in the glass surface; volume expansion of the corrosion products formed at the crack location did not cause the crack to propagate into the glass or cause fracturing of the glass around the corrosion pit.

1.4 SUMMARY

Seismic events can cause codisposal packages to impact emplacement pallets, drip shields, or other adjacent packages in the drifts. The bounding effects of these impacts on glass cracking are assessed by considering the range of calculated impact velocities of codisposal packages with adjacent packages. The effects of impacts within this range of velocities on glass cracking is assessed using experimental data that correlates the fractional increase in glass log cracking with impact velocities onto an unyielding surface. This shows that the fractional surface area increases are small and negligible for the more likely seismic events; even the more severe and unlikely seismic impacts cause only modest fractional surface area increases compared to the distribution range (4 to 17) for the nominal case. Therefore, use of the nominal case distribution range for the seismic case is appropriate.

The possible range of the exposure factor's value used in calculating the lower end of the $f_{exposure}$ range is 0 to 1. Use of a value of 0.5 is reasonable given the experimental evidence showing that use of a value near the upper end of the range would be overly conservative.

Additional glass cracking caused by volume expansion of glass corrosion products is not considered because available data indicate that glass corrosion at the location of a crack causes development of a wide pit in the glass rather than crack extension or additional glass fracturing and because experimental evidence for such a process is lacking.

2. COMMITMENTS TO NRC

None.

3. DESCRIPTION OF PROPOSED LA CHANGE

None.

4. REFERENCES

Bickford, D.F. and Pellarin, D.H. 1987. "Large Scale Leach Testing of DWPF Canister Sections." *Scientific Basis for Nuclear Waste Management X, Symposium held December 1-4, 1986, Boston, Massachusetts*. Bates, J.K. and Seefeldt, W.B., eds. 84, 509-518. Pittsburgh, Pennsylvania: Materials Research Society.

BSC (Bechtel SAIC Company) 2004. *Defense HLW Glass Degradation Model*. ANL-EBS-MD-000016 REV 02. Las Vegas, Nevada: Bechtel SAIC Company. ACC: DOC.20041020.0015; DOC.20050922.0002; LLR.20080408.0271; DOC.20081021.0002.

ENCLOSURE 2

Response Tracking Number: 00252-00-00

RAI: 3.2.2.1.3.4-003

Crovisier, J.L.; Honnorez, J.; and Eberhart, J.P. 1987. "Dissolution of Basaltic Glass in Seawater: Mechanism and Rate." *Geochimica et Cosmochimica Acta*, 51, (11), 2977-2990. Elmsford, New York: Pergamon.

Jiricka, A.; Vienna, J.D.; Hrma, P.; and Strachan, D.M. 2001. "The Effect of Experimental Conditions and Evaluation Techniques on the Alteration of Low Activity Glasses by Vapor Hydration." *Journal of Non-Crystalline Solids*, 292, (1-3), 25-43. New York, New York: North-Holland.

Pederson, L.R.; Buckwalter, C.Q.; and McVay, G.L. 1983. "The Effects of Surface Area to Solution Volume on Waste Glass Leaching." *Nuclear Technology*, 62, 151-158. Washington, D.C.: American Nuclear Society.

Perez, J.M., Jr. and Westsik, J.H., Jr. 1981. "Effects of Cracks on Glass Leaching." *Nuclear and Chemical Waste Management*, 2, 165-168. New York, New York: Pergamon Press.

SNL (Sandia National Laboratories) 2007. *Mechanical Assessment of Degraded Waste Packages and Drip Shields Subject to Vibratory Ground Motion*. MDL-WIS-AC-000001 REV 00. Las Vegas, Nevada: Sandia National Laboratories. ACC: DOC.20070917.0006; DOC.20080623.0002; DOC.20081021.0001.

Smith, T.H. and Ross, W.A. 1975. *Impact Testing of Vitreous Simulated High-Level Waste in Canisters*. BNWL-1903. Richland, Washington: Battelle Pacific Northwest Laboratories.

RAI Volume 3 Chapter 2.2.1.3.4, First Set, Number 4:

Justify the assumption that commercial SNF conditions will not be altered during transportation and/or interim storage.

Basis: In SAR 1.5.1.1.1 the applicant did not justify its assumptions that SNF conditions in the transportation, aging and disposal (TAD) canister would be unaltered at receipt. The applicant assumes that the conditions would not be altered during transportation and interim storage, or any alteration would not affect the commercial SNF performance in the repository.

During the transportation and interim storage, the commercial SNF matrix in the TAD canister may be hydrolyzed preferentially along grain boundaries (Finch, et al., 1999; Ahn and Mohanty, 2008) with residual moisture if there is no protection or even if only some cladding damage. This preferential hydration may lead to disintegration of the SNF matrix into grains. The grain boundary hydration could be facilitated if the TAD canister is not leak-tight and allows more moisture during the transportation and interim storage. The canister may not be leak-tight because of improper welding or the deterioration of welds during transportation. Additionally, the applicant did not address the conditions of high burnup SNF above 60 – 65 GWd/MTU. The fine-grained rim structure, which is enriched with plutonium, on the outer surface of the commercial SNF (NRC, 2007) may be subject to fracturing from vibration during transportation. The requested information is needed to verify compliance with 10 CFR 63.21(c)(3), (9), (12) and (14) and 63.114(a), (b) and (g).

1. RESPONSE

The assumption that commercial spent nuclear fuel (SNF) will not be altered during interim storage or transportation is based on requirements included in *Transportation, Aging and Disposal Canister System Performance Specification* (DOE 2008), which would allow for at-reactor loading and handling, on-site storage (at utility site), and off-site transportation of commercial SNF in compliance with applicable NRC regulations under 10 CFR Parts 50, 71, and 72. The requirements applicable to transportation, aging, and disposal (TAD) canister systems, in conjunction with NRC-issued certificates of compliance for independent storage of spent nuclear fuel, referred to in the RAI as interim storage and transportation, provide confidence that the TAD canisters will perform as intended. TAD canister systems, designed and used in accordance with their specifications, will not permit an unacceptable amount of moisture to enter during closure, drying, sealing, independent storage, and transportation. Therefore, the SNF condition assumed in the license application are valid. The effects of high burnup of commercial SNF have been accounted for in the degradation and transport analyses of the total system performance assessment (TSPA) analyses.

1.1 UTILITY REQUIREMENTS (INCLUDING QUALITY ASSURANCE)

Alteration of commercial SNF during transportation or independent storage is prevented by adhering to the requirements derived from the NRC regulations and guidance for independent storage and transportation. The implementation of the thermal and containment (structural) requirements for the canister and cask promulgated in the regulations will assure that the integrity of the commercial SNF is maintained during independent storage and transportation. At the time of transport to the repository, TAD canisters will have already been certified that they are acceptable for use for reactor site independent storage and transportation under 10 CFR Parts 71 and 72. As part of the NRC approval process, the following sections will be addressed: 10 CFR Part 71.55 (d)(2), the geometric form of the package contents should not become substantially altered under normal conditions of transport; and 10 CFR 72.122 (h)(1) provides that spent fuel cladding must be protected during storage against degradation that leads to gross ruptures or the fuel must be otherwise confined such that degradation of the fuel during storage will not pose operational safety problems with respect to its removal from storage. Based on the licensing requirements under Parts 71 and 72, DOE will rely upon the documentation of loading, storage, and transportation of individual TAD canisters prepared by the utility concurrent with such activity, as the basis for compliance with the repository-related design bases as previously discussed in the response to RAI Number 4.2.5.1-009, related to DOE quality assurance programs. Therefore, if the TAD canister satisfies its design bases, commercial SNF conditions would not be altered during reactor site independent storage and transportation.

Offsite activities and processes associated with the closure, at-reactor independent storage, and transportation of the commercial SNF loaded into a TAD canister are probable subjects of repository licensing specifications, as described in SAR Section 5.10. To ensure compliance with the TAD canister requirements, SAR Section 5.10, License Specifications, provides a discussion of administrative controls to be followed to authorize the use of TAD canisters. Specifically, SAR Table 5.10-3 describes a number of administrative controls to be included in the license specifications required by 10 CFR 63.43, including a proposed Canister and Transportation Cask Acceptance Program, which would impose restrictions on the receipt of TAD canisters or other shipping canisters to ensure conformance to repository requirements.

1.2 MOISTURE LIMITATIONS

The TAD canister system performance specification establishes requirements limiting the amount of residual moisture in closed TAD canisters and ensuring leak tightness following sealing of canisters. Examples of these performance requirements incorporated into the design and operations that assure that fuel alteration does not occur include:

- TAD canister leak testing processes to ensure containment integrity in accordance with ANSI N14.5-1997 (SAR Section 1.2.5);
- Closure requirements, including draining and drying of the TAD canister, in accordance with NUREG-1536 (NRC 1997) or NUREG-1567 (NRC 2000), which includes removing air and water (drying) and backfilling with inert gas to ensure verification of leak tightness (SAR Section 1.2.5.3.5.1);

- Final closure welds must meet the requirements of ISG-18 (NRC 2003b) to ensure no credible leakage (SAR Section 1.2.5.2.4.8 and SAR Table 1.2.5-2).

1.3 REPOSITORY REQUIREMENTS FOR COMMERCIAL SNF TO LIMIT STRUCTURAL OR THERMAL EFFECTS

At the repository, the performance characteristics of the TAD canister, as described in DOE 2008, apply to both the PCSA and the design of the surface handling facilities. They are also applied, as appropriate, as inputs to the TSPA analysis. These requirements, as specified in *Basis of Design for the TAD Canister Based Repository Design Concept* (BSC 2008) or *Project Design Criteria Document* (BSC 2009), are maintained from receipt to emplacement and are further specified for each surface facility and system that must receive or handle the canisters.

The TAD canister containment characteristics (performance requirements) are identified in SAR Section 1.5.1.1.1.2.6.1.2. The TAD canister thermal characteristics (performance requirements) are identified in SAR Section 1.5.1.1.1.2.5.3.

Thermal requirements imposed on handling operations are consistent with the requirements of 10 CFR Parts 71 and 72 to limit thermally induced effects.

Handling requirements are consistent with the requirements of 10 CFR Parts 71 and 72 to remain within the structural analysis bases.

With respect to high burnup fuel fracture, the TAD canister will demonstrate compliance with requirements of 10 CFR Parts 71 and 72 for fuel with up to 80 GWd/MTU for pressurized water reactor commercial SNF and up to 75 GWd/MTU for boiling water reactor commercial SNF. No less than 5 years out-of-reactor cooling time is required for both fuel types. It is noted that NRC has indicated that approval of greater than 45 GWd/MTU would be reviewed on a case-by-case basis, therefore, initial limitations of 45 GWd/MTU may be imposed by the NRC on the TAD canister, consistent with current NRC guidance in NUREG-1536 (NRC 1997), NUREG-1567 (NRC 2000a), and NUREG-1617 (NRC 2000b). Prior to the use of any transportation cask at the repository, analyses will be performed to demonstrate compliance with the Yucca Mountain Project repository-specific criteria and repository nuclear safety design bases (SAR Section 1.2.8.4.5.1).

1.4 EFFECTS ON THE TSPA DUE TO HIGH BURNUP

At burnup higher than approximately 45 GWd/MTU, a “rim region” (150 to 250 µm thick) is formed at the outer surface of the pellets, characterized by a very fine-grained fuel microstructure, up to 10% to 15% porosity, and local burnup as much as three times higher than the pellet average burnup (BSC 2004, p. 6-2). Further alteration of this rim region, in higher burnup fuels, such as fracture from vibration during transportation, is also not expected, because the fuel and cladding are intimately bonded in high burnup fuel.

Nonetheless, the effects of these microstructural features of commercial SNF (particularly the effects of the connected porosity) on the specific surface area of commercial SNF are accounted

for in the uncertainty distribution of the effective surface area discussed in *CSNF Waste Form Degradation: Summary Abstraction* (BSC 2004, Section 6.4.1.5). The effective specific surface area spans a range of 3.9×10^{-3} to $4.7 \times 10^{-5} \text{ m}^2/\text{g}$. Analyses reported in *Total System Performance Assessment Model/Analysis for the License Application* (SNL 2008, Appendix K) confirm that the uncertainty in the commercial SNF-specific surface area is not influential to the outcome of the performance assessment. In particular, uncertainty in the commercial SNF-specific surface area has no effect on the magnitude of, or uncertainty in, estimates of mean dose to the reasonably maximally exposed individual, which is compared to the individual protection standard specified at 10 CFR 63.311.

During the postclosure period, in postulated exposure of the oxidized fuel to humid air, few, if any, submicrometer particles are expected to be available for suspension as colloids. Based on the above considerations, exposure of commercial SNF to “dry” air oxidizing conditions followed by exposure to humid air is unlikely to lead to formation of submicrometer particles that would be available for suspension as colloids when water contacts the oxidized fuel (SNL 2007, Section 6.3.6).

2. COMMITMENTS TO NRC

None.

3. DESCRIPTION OF PROPOSED LA CHANGE

None.

4. REFERENCES

ANSI N14.5-1997. 1998. *American National Standard for Radioactive Materials—Leakage Tests on Packages for Shipment*. New York, New York: American National Standards Institute. TIC: 247029.

BSC (Bechtel SAIC Company) 2004. *CSNF Waste Form Degradation: Summary Abstraction*. ANL-EBS-MD-000015 REV 02. Las Vegas, Nevada: Bechtel SAIC Company. ACC: DOC.20040908.0001; DOC.20050620.0004.

BSC 2008. *Basis of Design for the TAD Canister-Based Repository Design Concept*. 000-3DR-MGR0-00300-000-003. Las Vegas, Nevada: Bechtel SAIC Company. ACC: ENG.20081006.0001.

BSC 2007. *Project Design Criteria Document*. 000-3DR-MGR0-00100-000-007 CBCN 013. Las Vegas, Nevada: Bechtel SAIC Company. ACC: ENG.20071016.0005; ENG.20071108.0001; ENG.20071220.0003; ENG.20080107.0001; ENG.20080107.0002; ENG.20080107.0016; ENG.20080107.0017; ENG.20080131.0006; ENG.20080305.0002; ENG.20080305.0011; ENG.20080305.0012; ENG.20080306.0009; ENG.20080313.0004; ENG.20080710.0001.

DOE (U.S. Department of Energy) 2008. *Transportation, Aging and Disposal Canister System Performance Specification*. WMO-TADCS-000001, Rev. 1 ICN 1. Washington, D.C.: U.S.

Department of Energy, Office of Civilian Radioactive Waste Management. ACC: DOC.20080331.0001.

NRC (U.S. Nuclear Regulatory Commission) 1997. *Standard Review Plan for Dry Cask Storage Systems*. NUREG-1536. Washington, D.C.: U.S. Nuclear Regulatory Commission. ACC: MOL.20010724.0307.

NRC 2000a. *Standard Review Plan for Spent Fuel Dry Storage Facilities*. NUREG-1567. Washington, D.C.: U.S. Nuclear Regulatory Commission. TIC: 247929.

NRC 2000b. *Standard Review Plan for Transportation Packages for Spent Nuclear Fuel*. NUREG-1617. Washington, D.C.: U.S. Nuclear Regulatory Commission. TIC: 249470.

NRC 2003a. *Interim Staff Guidance-11, Revision 3. Cladding Considerations for the Transportation and Storage of Spent Fuel*. ISG-11, Rev. 3. Washington, D.C.: U.S. Nuclear Regulatory Commission. ACC: MOL.20040721.0065.

NRC 2003b. *Interim Staff Guidance-18. The Design/Qualification of Final Closure Welds on Austenitic Stainless Steel Canisters as Confinement Boundary for Spent Fuel Storage and Containment Boundary for Spent Fuel Transportation*. ISG-18. Washington, D.C.: U.S. Nuclear Regulatory Commission. TIC: 254660.

SNL (Sandia National Laboratories) 2007. *Waste Form and In-Drift Colloids-Associated Radionuclide Concentrations: Abstraction and Summary*. MDL-EBS-PA-000004 REV 03. Las Vegas, Nevada: Sandia National Laboratories. ACC: DOC.20071018.0019; LLR.20080325.0281.

SNL 2008. *Total System Performance Assessment Model /Analysis for the License Application*. MDL-WIS-PA-000005 REV 00 AD 01. Las Vegas, Nevada: Sandia National Laboratories. ACC: DOC.20080312.0001; LLR.20080414.0037; LLR.20080507.0002; LLR.20080522.0113; DOC.20080724.0005; DOC.20090106.0001.

RAI: Volume 3, Chapter 2.2.1.3.4, First Set, Number 5:

Assess the effects and significance on abstracted glass waste form pH limits (i.e., Cell 1a pH limits illustrated in SAR Figure 2.3.7-20) of using the 5-DHLW/DOE Long design to represent codisposal waste packages in the in-package chemistry model.

Basis: The applicant selected the 2-MCO/2-DHLW design to represent Cell 1a and Cell 1b of codisposal waste packages for developing in-package pH abstractions for TSPA (SAR Section 2.3.7.5.3). However, the most common codisposal waste package is the 5-DHLW/DOE Long, which contains 5 HLW glass canisters instead of the 2 HLW glass canisters in the 2-MCO/2-DHLW design. The applicant has identified dissolution of glass waste as a process capable of generating high pH inside waste packages (SAR Sections 2.3.7.5.1 and 2.3.7.5.3.1). The more abundant and glass-rich 5-DHLW/DOE Long design would provide greater glass surface area to react with incoming waters and, therefore, could potentially increase the maximum abstracted pHs for Cell 1a, which in turn could increase release rates. The requested information is needed to verify compliance with 10 CFR 63.21(c)(3), (9), and (11)-(14) and 10 CFR 63.114(b) and (c).

1. RESPONSE

The approach used to establish the pH limits is shown to be unaffected by the choice of waste package design (2-MCO/2-DHLW instead of 5-DHLW/DOE Long) because the pH limits are based on buffering reactions that are unaffected by the waste package choice.

1.1 EFFECTS OF CODISPOSAL WASTE PACKAGE DESIGN ON pH LIMITS

The in-package chemistry (IPC) model is a single cell batch reactor model. One of its purposes is to establish the waste form cell pH limits for the total system performance assessment (TSPA). These limits are based on the effects of specific reactions that buffer pH. The IPC model is also used to predict the pH in the cell over time for specific sets of inputs, but these pH predictions are not used by the TSPA, except to show that the pH remains within the pH limits established by the buffering reactions.

For Cell 1a, the IPC model simulates the two HLW glass-pour canisters of the 2-MCO/2-DHLW waste package instead of the five HLW glass-pour canisters of the 5-DHLW/DOE Long waste package. If the IPC model for Cell 1a had instead used the 5-DHLW/DOE Long design, the only differences in the reactants would have been the total volumes of glass and Stainless Steel Type 304L in Cell 1a, each of which would have been 2.5 times larger (five canisters instead of two). The void volume and total surface areas of the reactants would also have been larger by a factor of 2.5.

Each IPC simulation was scaled to one liter of water. If the proportions of volume and surface area of each reactant, including water, are identical, the concentration-based results of the IPC

model (e.g., pH, ionic strength, and aqueous species concentrations) will be the same regardless of the initial total volumes and surface areas of the reactants. Thus, if Cell 1a had been composed of five HLW glass-pour canisters instead of two, and the total volume of water in the cell had also been 2.5 times larger than the volume of water for two canisters, there would have been no change in the IPC model results.

If instead, the amount of water in the cell had been held constant but the cell size had been increased to that of the 5-DHLW/DOE Long waste package, then the initial ratio of water to reactants would have decreased. While this decrease would have changed the IPC predictions of pH over time, it would not have changed the pH limits. The pH limits predicted by the IPC model are the only pH parameters relevant to the TSPA model.

1.2 pH LIMITS IN HLW GLASS CANISTERS

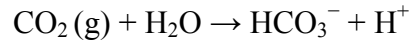
1.2.1 pH Effects of HLW Glass Degradation

In a system with no competing reactions, degradation of HLW glass in pure water is predicted to produce an alkaline solution consisting of the following principal ions: Na^+ , HSiO_3^- , Li^+ , BO_2^- , and OH^- . For base case conditions, the glass degradation rate in the HLW glass waste form cell is approximately 2.6×10^{-12} molal/s. This rate is based on a most likely fracture exposure factor of 4, a void volume half-filled with water, and no dry reactant surfaces. At this rate, HLW glass degradation is predicted to generate alkalinity at the rate of 5.8×10^{-5} molal/yr.

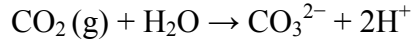
A maximum degradation rate of about three orders of magnitude higher can be estimated assuming maximum measured rates, a maximum fracture exposure factor of 17 (SNL 2007, Section 4.1.3.3), and a lower water saturation that would still permit all surfaces to be contacted by water. However, degradation rates near these maximum values are not expected to be realistic for the longer time scale of the TSPA calculations based on the results of long-term tests.

1.2.2 Upper pH Limit

Over a pH range of approximately 6.3 to 10.3 at 25°C (6.4 to 10.1 at 100°C), dissolution of carbon dioxide in water produces both dissolved carbonate and acidity via this reaction:



Above a pH of about 10.3, the predominant reaction is:



Due to the acidity imparted by these reactions, dissolution of carbon dioxide is predicted to establish the upper pH limit in Cell 1a. The rate at which carbon dioxide dissolves into Cell 1a water is expected to be rapid compared to the rate of glass degradation.

IPC model titration simulations indicate that carbon dioxide provides a highly effective buffer to sources of alkalinity, even for an alkalinity production rate as high as 5×10^{-2} molal/yr

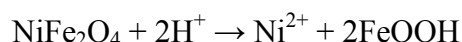
(e.g., SNL 2007, Figure 6-39[a]). Because there is a vast reservoir of carbon dioxide, there is essentially no relevant limit to the buffering capacity of carbon dioxide. Thus, the pH limits were established assuming a maximum bounding alkalinity production rate of 5×10^{-2} molal/yr (SNL 2007, Section 6.10.1.1[a]).

To establish the pH limits for the TSPA, the IPC titration calculations were performed over the expected ranges of carbon dioxide partial pressure and ionic strength. These limits are shown in SAR Figure 2.3.7-20. Details of these calculations are provided in the supporting documentation (SNL 2007, Section 6.10.1[a]).

Had the 5-DHLW/DOE Long waste package been used to define the Cell 1a contents, the alkalinity production rate of the HLW glass dissolution would have been the same, and therefore the upper pH limit calculations would have been identical. If instead, the volume of water were not allowed to increase along with the volumes of materials, the water saturation would have decreased from 50% to 20% and the base case alkalinity production rate would have increased from 5.8×10^{-5} molal/yr to 1.4×10^{-4} molal/yr. This rate is well below the rate at which carbon dioxide dissolution would buffer the alkalinity generated by glass dissolution; therefore, there would still be no effect on the upper pH limits calculated.

1.2.3 Lower pH Limit

The accumulation of corrosion products buffers the sources of acidity in Cell 1a. As the Stainless Steel Type 304L degrades, the IPC model predicts that trevorite (NiFe_2O_4) will precipitate. Trevorite, an established corrosion product of stainless steel, represents the accumulation of nickel-iron oxides in the model (SNL 2007, Section 6.3.4.1[a]). If processes cause pH to decrease below approximately 5.5, trevorite is predicted to convert to goethite (FeOOH), releasing nickel as Ni^{2+} and consuming two protons for each nickel atom released (SNL 2007, Section 6.3.4.1[a]):



This reaction is consistent with the increase in nickel solubility as pH falls below 6. This reaction buffers pH because the consumption of protons resists the pH decrease.

The buffering of this reaction and the associated pH minimum is quantified by titrating the system with acid (SNL 2007, Section 6.10.1[a]). Below a pH of 6 in the presence of trevorite, the pH will slowly decrease for each aliquot of acid added. Only after trevorite is completely dissolved by the acid will the pH decrease quickly with additional aliquots of acid. The minimum pH that can be reached while trevorite is present (i.e., the lower pH limit established for the TSPA) is the pH immediately prior to the complete dissolution of trevorite.

Based on the titration calculations, the precipitation of trevorite in Cell 1a provides acid-neutralizing capacity (ANC) at a rate of approximately 0.001 molal/yr under base-case conditions (SNL 2007, Section 6.10.1.1[a]). This rate is more than 30 times higher than the acid production rate of the only major internal source of acidity in Cell 1a, the degradation of Stainless Steel Type 304L (3×10^{-5} molal/yr under base-case conditions). Because the

degradation of stainless steel produces the major internal sources of both the ANC and acidity, and because it produces ANC much faster than acidity, the ANC will not be exhausted by internal sources of acidity. Dissolution of carbon dioxide is not a major source of acidity in this case because in this pH range it generates carbonic acid, a weak acid that does not provide significant acidity under acidic conditions. Incoming seepage water is also not expected to provide acidity at a rate that would be required to exceed the ANC production rate (SNL 2007, Section 6.10.1[a]). Therefore, the trevorite titration simulations are appropriate for calculating the lower pH limits for this cell. Because the lower pH limits for this cell depend only on the degradation of Stainless Steel Type 304L, which is present in both 2-MCO/2-DHLW and 5-DHLW/DOE Long codisposal waste packages, they are also insensitive to the codisposal waste package modeled.

1.3 SUMMARY

The use of the 2-MCO/2-DHLW waste package design instead of the 5-DHLW/DOE Long waste package design has no effect on the pH limits of the HLW glass waste form cell (Cell 1a). The pH limits of Cell 1a are based on buffering reactions that will be unaffected by the choice of codisposal waste package.

2. COMMITMENTS TO NRC

None.

3. DESCRIPTION OF PROPOSED LA CHANGE

None.

4. REFERENCES

SNL (Sandia National Laboratories) 2007. *In-Package Chemistry Abstraction*. ANL-EBS-MD-000037 REV 04 ADD 01. Las Vegas, Nevada: Sandia National Laboratories.
ACC: DOC.20070816.0004; DOC.20051130.0007; LLR.20080325.0276;
DOC.20081120.0004^a.

NOTE: ^aProvided as an enclosure to letter from Williams to Sulima dtd 02/17/2009. "Yucca Mountain – Request for Additional Information Re: License Application (Safety Analysis Report Section 2.1), Safety Evaluation Report Volume 3 – Postclosure Chapters 2.2.1.1 and 2.2.1.3.7 – Submittal of Department of Energy Reference Citations"

RAI Volume 3, Chapter 2.2.1.3.4, First Set, Number 6:

Provide support to address predicted high ionic strength conditions in the waste form cells resulting from in-package chemistry model simulations.

Basis: The applicant provided support for the in-package chemistry model by showing that predicted secondary phases and pH ranges are consistent with observations from natural soils and groundwater, natural analogues, and/or laboratory experiments (SAR Section 2.3.7.5.3.2). However, SAR Section 2.3.7.5.3.2 does not include support for predicted ionic strength conditions. Ionic strength abstractions generated from the results of in-package chemistry model simulations are used in TSPA to determine the stability of colloids (e.g., colloid suspensions are unstable at high ionic strengths). High ionic strengths, predicted in the waste form cells based on in-package chemistry model simulations (SAR Figures 2.3.7-22 through 2.3.7-25), weaken repulsive forces between colloids, causing colloidal suspensions to become unstable and settle out of solution, decreasing overall release rates. Therefore, it is important that model support for predicted high ionic strength conditions resulting from in-package chemistry model simulations are addressed in the SAR. The requested information is needed to verify compliance with 10 CFR 63.21(c)(15) and 10 CFR 63.114(g).

1. RESPONSE

Observations from laboratory experiments and groundwater samples are consistent with the in-package chemistry (IPC) liquid influx model relationship between ionic strength and flow rate. In addition, ionic strength under low flow rate conditions is controlled by the IPC vapor influx model when the relative humidity is sufficiently high.

1.1 SUPPORT FOR IN-PACKAGE CHEMISTRY IONIC STRENGTH PREDICTIONS

Confidence is built in the IPC model by demonstrating that the predictions of secondary phases are correct, and that the predicted pH ranges are consistent with those observed in qualitatively similar soils and groundwaters (SNL 2007a, Section 7.4[a]). These demonstrations provide indirect support for the IPC ionic strength predictions. More direct support of the IPC ionic strength predictions is provided below.

The IPC model consists of two submodels—a liquid influx model and a vapor influx model (SNL 2007a, Section 6.3[a]). The liquid influx model simulates the effects of liquid water flowing into the waste form cell. The vapor influx model simulates the effects of waste package relative humidity.

1.1.1 Liquid Influx Model

In the IPC liquid influx model, low flow rates through the waste form cells can generate high ionic strengths resulting from the degradation of commercial spent nuclear fuel (SNF), high-level waste (HLW) glass, and stainless steel (SAR Figures 2.3.7-22 to 2.3.7-24). When high ionic

strengths are predicted, low flow rates provide sufficient residence time for significant buildup in solution of soluble degradation products, such as sodium and nitrate, and/or significant consumption of H₂O via degradation reactions, such as the oxidation of UO₂ to schoepite (SNL 2007a, Section 6.10.1.1[a]).

This relationship between ionic strength and residence time is supported by the occurrence of ground water brines in crystalline rocks. For example, brines deep in Canadian Shield granite appear to be primarily derived from millions of years of slow igneous rock dissolution in the presence of ancient rainwater (Appelo and Postma 1994, Section 8.1.2). Thus, the general cause of the high ionic strengths predicted by the IPC liquid influx model for long contact times (low flow rates) is consistent with the general cause attributed to the high ionic strengths observed in the deep brines of crystalline rocks. It is also consistent with general models that relate low flow rates to increased aqueous concentrations when dissolution rates are low (e.g., Freeze and Cherry 1979, Section 7.8 and Figure 7.17).

Additional support of the ionic strength predictions in the commercial SNF cell is provided by 10 years of measurements from UO₂ alteration experiments (Wronkiewicz et al. 1996). In these experiments there were two different rates of simulated ground water injections, 0.075 mL every 3.5 days and 0.0375 mL every 7 days (Wronkiewicz et al. 1996, p. 82). These rates are equivalent to 7.82 mL/yr and 1.95 mL/yr. The UO₂ pellets in the experiments occupied total volumes of approximately 2 to 5 mL. Considering that the volumes of commercial SNF in the waste form cells simulated in the total system performance assessment for the license application (TSPA-LA) model were approximately 1,100 L, the experimental flow rates were equivalent to waste form cell flow rates between approximately 500 and 4,000 L/yr. The IPC liquid influx model predicts that flow rates this high over 10 years will not lead to high ionic strength (SAR Figure 2.3.7-22). This prediction is consistent with the small changes in ionic strength indicated by the results of the UO₂ alteration experiments (Wronkiewicz et al. 1996, Figure 5 and Sections 4.1.2 and 4.1.3).

Further support of the IPC liquid influx model ionic strength predictions is provided by a PHREEQC simulation of the CSNF base case that was performed as part of the IPC model validation process (SNL 2007a, Section 7.10.1[a]). PHREEQC is a United States Geological Service (USGS) code that has many of the same features as EQ6, the code used to execute the IPC model. Although the two codes differ in how they execute a flow-through cell simulation, each of the processes simulated by EQ6 in the model can be simulated using PHREEQC. Each simulation used the thermodynamic database of the IPC model. The results of the PHREEQC simulation indicated negligible differences from the EQ6 code in the predictions of pH and ionic strength over time (SNL 2007a, Figures 7-1[a] and 7-2[a]). These results provide confidence that the IPC mathematical model, as executed by EQ6, performs as intended.

1.1.2 Vapor Influx Model

In the IPC vapor influx model, exchange of water between the gas phase of the drift and the liquid phase in the waste form cell is rapid enough to maintain a chemical activity of water in solution that is equivalent to the relative humidity expressed as a fraction (SNL 2007a, Section 6.3[a]). The driving force for this equilibration process is the osmotic potential of the

solution. By using relative humidity to effectively establish the amount of vapor influx, the IPC vapor influx model uses an equilibrium endpoint to provide the thermodynamically favored ionic strength.

The relationship between the activity of water and ionic strength is strong. Like ionic strength, the activity of water is a function of the molalities of dissolved constituents. The predicted IPC model relationships between ionic strength and relative humidity are shown for each waste form cell in SAR Figure 2.3.7-25 for relative humidity above 98%. These predictions were generated by adjusting the activity of water (effectively, the equilibrium relative humidity) in the waste form cells and allowing the rapid reactions (aqueous speciation, gas exchange, and precipitation and dissolution of secondary minerals) to equilibrate in response to the adjustments. These predictions demonstrate that the relationship between relative humidity and ionic strength is not highly sensitive to the particular waste form cell simulated.

The ionic strength results for this relative humidity range (98% to 100%) are supported by predictions of the in-drift precipitates/salts (IDPS) model for a wide range of salt solutions (SNL 2007a, Figure 6-50[a]). The IDPS model uses a Pitzer database to simulate aqueous geochemical reactions for solutions with ionic strengths up to 10 molal and higher. The applicability of the IDPS model for ionic strength predictions below one molal is, in turn, supported by a validation simulation that used the same database and activity equations used by the IPC model. That simulation produced ionic strength predictions up to one molal that were nearly identical to the IDPS model predictions (SNL 2007b, Section 7.3).

The IDPS model predictions for simple salt solutions were used to extend the IPC model relative humidity–ionic strength relationships for each waste form cell down to 95% relative humidity (SNL 2007a, Section 6.10.2.2[a]). The trends predicted by the IDPS model and adopted by the IPC model are further supported by simulations that show that the IDPS model accurately predicts the activity of water (equilibrium relative humidity) for salt solutions containing excess solid-phase salts (SNL 2007b, Section 7.1.1.1.2).

1.1.3 Controls for High Ionic Strength

For each time step, the TSPA-LA model uses the lower of the two ionic strengths predicted by the liquid influx and vapor influx models (SNL 2007a, Section 6.10.9.1[a]). Therefore, the high ionic strengths predicted by the liquid influx model (SAR Figures 2.3.7-22 to 2.3.7-24) can only occur if the vapor influx model predicts a higher ionic strength. The vapor influx model sets a reasonable upper limit for ionic strength because vapor influx is rapid compared to the low flow rates of the liquid influx model that cause high ionic strength.

1.2 SUMMARY

High ionic strength conditions are predicted by the IPC liquid influx model when flow rates through the waste form cell are low. This inverse relationship between ionic strength and flow rate is consistent with general models of slow mineral dissolution in groundwater, the analysis of the evolution of deep Canadian Shield brines, and the results of UO₂ alteration experiments. When the waste package relative humidity is sufficiently high, vapor influx prevents attainment

of the high ionic strength predictions of the liquid influx model. Thus, when the IPC vapor influx model predicts a lower ionic strength than the IPC liquid influx model, the lower ionic strength of the vapor influx model is used by the TSPA-LA model.

2. COMMITMENTS TO NRC

None.

3. DESCRIPTION OF PROPOSED LA CHANGE

None.

4. REFERENCES

Appelo, C.A.J. and Postma, D. 1994. *Geochemistry, Groundwater and Pollution*. Brookfield, Vermont: A.A. Balkema.

Freeze, R.A. and Cherry, J.A. 1979. *Groundwater*. Englewood Cliffs, New Jersey: Prentice-Hall.

SNL (Sandia National Laboratories) 2007a. *In-Package Chemistry Abstraction*. ANL-EBS-MD-000037 REV 04 ADD 01. Las Vegas, Nevada: Sandia National Laboratories.

ACC: DOC.20070816.0004; DOC.20051130.0007; LLR.20080325.0276;
DOC.20081120.0004^a.

SNL 2007b. *In-Drift Precipitates/Salts Model*. ANL-EBS-MD-000045 REV 03. Las Vegas, Nevada: Sandia National Laboratories. ACC: DOC.20070306.0037; LLR.20080401.0242; DOC.20080707.0001.

Wronkiewicz, D.J.; Bates, J.K.; Wolf, S.F.; and Buck, E.C. 1996. "Ten-Year Results from Unsaturated Drip Tests with UO₂ at 90°C: Implications for the Corrosion of Spent Nuclear Fuel." *Journal of Nuclear Materials*, 238, (1), 78-95. Amsterdam, The Netherlands: North-Holland.

NOTE: ^aProvided as an enclosure to letter from Williams to Sulima dtd 02/17/2009. "Yucca Mountain – Request for Additional Information Re: License Application (Safety Analysis Report Section 2.1), Safety Evaluation Report Volume 3 – Postclosure Chapters 2.2.1.1 and 2.2.1.3.7 – Submittal of Department of Energy Reference Citations"

RAI Volume 3, Chapter 2.2.1.3.4, First Set, Number 7:

Provide justification for excluding available pH data from glass dissolution experiments to support predicted HLW glass waste form pH ranges resulting from in-package chemistry model simulations.

Basis: The applicant provided support for the in-package chemistry model in SAR Section 2.3.7.5.3.2. The applicant supported abstracted pH ranges for the HLW glass waste form (i.e., Cell 1a represented by 2-DHLW) generated by in-package model simulations by comparison to pH ranges observed in groundwater in contact with basalt and basalt glass. However, abstracted pH ranges for the HLW glass waste form were not compared to available data from glass dissolution experiments (Bates et al., 1994; Jantzen et al., 1993). The pHs reported in these glass dissolution experiments had relatively high pHs (pH > 10). Because high pH contributes to processes that are risk significant to waste isolation (i.e., neptunium solubility), it is important that predicted pH ranges in the HLW glass waste form cell be adequately addressed and justified in the model. The requested information to verify compliance with 10 CFR 63.21(c)(15) and 10 CFR 63.114(g).

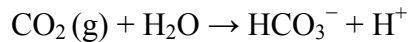
1. RESPONSE

The pH in Cell 1a (i.e., the cell containing glass in the codisposal -2-MCO/2-DHLW packages) is strongly influenced by the CO₂ fugacity, as presented in SAR Figure 2.3.7-20. Dissolution of CO₂ is expected to control the upper end of the pH range in Cell 1a. Because the cited glass dissolution tests are closed system tests, their measured pH values are controlled by the relative release rates of alkaline and pH buffering components from the glass as it corrodes. The pH values measured in these tests do not account for the effect of the CO₂ dissolution, which is the process that is expected to control the upper end of the pH range in the open repository system. Consequently, it is not appropriate to compare the pH values measured in these tests to the ranges calculated by the in-package chemistry model for Cell 1a in the codisposal packages and not using these pH data to support the pH range resulting from in-package chemistry model simulations is justified.

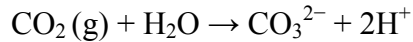
1.1 EFFECTS OF CARBON DIOXIDE ON CALCULATED UPPER pH LIMIT

The in-package chemistry (IPC) model is used to calculate the pH limits in Cell 1a (i.e., the cell containing glass in the codisposal packages) for the total system performance assessment (TSPA). The upper limit of the range is based on the effects of reactions that buffer and limit the upper end of the pH range in the glass cell.

In the open repository system, dissolution of carbon dioxide is expected to limit the upper end of the pH range. Over a pH range of approximately 6.3 to 10.3 at 25°C (6.4 to 10.1 at 100°C), dissolution of carbon dioxide in water produces dissolved carbonate and acidity via the reaction:



Above a pH of about 10.3, the predominant reaction is:



Due to the acidity imparted by these reactions, dissolution of carbon dioxide is predicted to establish the upper pH limit in Cell 1a. The rate at which carbon dioxide dissolves into Cell 1a water is expected to be rapid compared to the rate of glass degradation.

For base case conditions, the glass degradation rate in the high-level waste (HLW) glass waste form cell is approximately 2.6×10^{-12} molal/s. This rate is based on a most likely fracture exposure factor of 4, a void volume half-filled with water, and no dry reactant surfaces. At this rate, HLW glass degradation generates alkalinity at the rate of 5.8×10^{-5} molal/yr.

A maximum degradation rate of about three orders of magnitude higher (i.e., an alkalinity production rate of about 6×10^{-2} molal/yr) can be estimated assuming maximum measured rates, a maximum fracture exposure factor of 17, and a lower water saturation that would still permit all surfaces to be contacted by water. However, degradation rates near these maximum values are unlikely for the longer time scale of the TSPA calculations based on the results of long-term tests.

IPC model titration simulations indicate that carbon dioxide buffers the pH and controls the upper end of the pH range in Cell 1a, even for an alkalinity production rate as high as 5×10^{-2} molal/yr (e.g., SNL 2007, Figure 6-39[a]). Because there is a vast reservoir of carbon dioxide, there is essentially no relevant limit to the buffering capacity of carbon dioxide. Thus, the pH limits were established assuming a maximum alkalinity production rate of 5×10^{-2} molal/yr (SNL 2007, Section 6.10.1.1[a]).

To establish the pH limits for the TSPA, the IPC titration calculations were performed over the expected ranges of carbon dioxide partial pressure and ionic strength. These limits are shown in SAR Figure 2.3.7-20. Details of these calculations are provided in the supporting documentation (SNL 2007, Section 6.10.1[a]).

1.2 FACTORS CONTROLLING pH MEASURED IN HLW GLASS TESTS

The tests cited in the RAI are closed system tests for which there is a negligible influence of carbon dioxide dissolution on the measured pH values. The glass testing described by Jantzen et al. (1993) involves product consistency tests (PCTs) conducted on the “environmental assessment (EA) benchmark” glass. These PCTs were conducted at 90°C in closed vessels using crushed glass powders (100 to 200 mesh) and a volume of pure water to achieve a nominal ratio of the glass sample surface area (S) to solution volume (V) of $2,000 \text{ m}^{-1}$. Likewise, the 2,000 and $20,000 \text{ m}^{-1}$ glass tests for which pH results are presented in Figure 2-18 of the report by Bates et al. (1994) (reference cited in the RAI) were also PCTs conducted at 90°C in closed vessels; the 10 m^{-1} tests were also conducted at 90°C in closed vessels but used lower surface area monolithic samples to achieve the target 10 m^{-1} S/V ratio.

Degradation of HLW glass in pure water is predicted to produce an alkaline solution consisting of the following principal ions: Na^+ , HSiO_3^- , Li^+ , BO_2^- , and OH^- . The pH depends on the combined effects of the relative release of alkali compared to the release of the buffering silicate and borate components of the glass. Sodium, potassium, and lithium released from the glass drives the solution basic as a result of hydrogen ion exchange for these alkali metal ions in the glass. The release of silicate and borate components buffer the pH and limit the pH excursion (Pederson et al. 1983, p. 154) under these closed system test conditions. As illustrated in Figure 2-18 of the report by Bates et al. (1994), the measured pH depends on the S/V ratio at which the test is conducted. The pH increases as the ratio of glass sample surface area (S) to the volume of the test solution (V) increases. In tests using glass powder samples, the initial rapid alkali release from the outer surface of high surface area powders into relatively small solution volumes, when compared to the relatively slow initial release of the silicate and borate buffering components, causes an initially rapid increase in pH values observed in the tests. However, at a later stage in the reaction progress, when the fractional release of the buffering components is comparable to that of alkali, the pH attains a steady state or decreased value (Pederson et al. 1983, p. 155; Bates et al. 1994, Figure 2-18) that is controlled by the combined effects of the released alkali and buffering components of the glass.

1.3 SUMMARY

Dissolution of CO_2 is expected to control the upper end of the pH range in Cell 1a. In contrast, relative release rates of alkaline and pH buffering components control the pH observed by Bates et al. (1994) and Jantzen et al. (1993). Consequently, it is not appropriate to compare the pH values measured in these tests to the ranges calculated by the IPC model for Cell 1a in the codisposal packages because the processes that control the pH are different.

2. COMMITMENTS TO NRC

None.

3. DESCRIPTION OF PROPOSED LA CHANGE

None.

4. REFERENCES

Bates, J.K., C.R. Bradley, E.C. Buck, J.C. Cunnane, W.L. Ebert, X. Feng, J.J. Mazer, D.J. Wronkiewicz, J. Sproull, W. L. Bourcier, B. P. McGrail, and M.K. Altenhofen 1994. "High-Level Waste Borosilicate Glass A Compendium of Corrosion Characteristics Volume 2." *DOE-EM-0177 Vol. 2 of 3*. Washington, DC: Department of Energy.

Jantzen, C.M., N.E. Bibler, D.C. Beam, C.L. Crawford, and M.A. Pickett 1993. "Characterization of the Defense Waste Processing Facility (DWPF) Environmental Assessment (EA) Glass Standard Reference Material (U)." *WSRC-TR-92-346, Revision 1*. Aiken SC: Westinghouse Savannah River Company.

ENCLOSURE 6

Response Tracking Number: 00256-00-00

RAI: 3.2.2.1.3.4-007

Pederson, L.R.; Buckwalter, C.Q.; and McVay, G.L. 1983. "The Effects of Surface Area to Solution Volume on Waste Glass Leaching." *Nuclear Technology*, 62, 151-158. Washington, D.C.: American Nuclear Society.

SNL (Sandia National Laboratories) 2007. *In-Package Chemistry Abstraction*. ANL-EBS-MD-000037 REV 04 ADD 01. Las Vegas, Nevada: Sandia National Laboratories.
ACC: DOC.20070816.0004; DOC.20051130.0007; LLR.20080325.0276;
DOC.20081120.0004^a.

NOTE: ^aProvided as an enclosure to letter from Williams to Sulima dtd 02/17/2009. "Yucca Mountain – Request for Additional Information Re: License Application (Safety Analysis Report Section 2.1), Safety Evaluation Report Volume 3 – Postclosure Chapters 2.2.1.1 and 2.2.1.3.7 – Submittal of Department of Energy Reference Citations"

RAI Volume 3, Chapter 2.2.1.3.4, First Set, Number 8:

Provide justification for the approach in which pH is computed in the three EBS radionuclide transport domains (waste form, corrosion products, and invert) using unrelated abstractions. Provide justification that this approach does not potentially lead to underestimating EBS release rates.

Basis: Within the EBS component of TSPA, pH is calculated separately in Cell 1 (waste form domain), Cell 2 (corrosion products domain), and the invert. In Cell 1, pH is sampled from a range that depends on (i) package type, (ii) vapor or liquid influx conditions, (iii) ionic strength, and (iv) CO₂ partial pressure (SNL, 2008, Section 6.3.7.2.2). In Cell 2, pH is calculated from a formula that involves CO₂ partial pressure and the aqueous U concentration (SAR Section 2.3.7.5.3.1). The invert pH is obtained from the seepage evaporation abstraction (SAR Section 2.3.5.5). There is no integration of abstracted pH as water flows from the waste package to the invert. Therefore, concentration limits and colloid stabilities, some of which depend strongly on pH, can vary markedly from one cell to another within a single realization. The requested information is needed to verify compliance with 10 CFR 63.21(c)(9), (11)-(15) and 63.114(a), (b), and (g).

1. RESPONSE

The three Engineered Barrier System (EBS) radionuclide transport domains have pH abstractions that are a set of physically distinct representations and are appropriately linked or correlated to their upstream domains, and thus the abstractions do not lead to potential underestimation of radionuclide release from the EBS. As stated in the RAI, the domains are represented in the total system performance assessment (TSPA) model by three reaction “cells” that relate to the waste form domain, corrosion products domain, and the invert.

The pH of seepage or condensation fluid entering and traveling through a waste package, and the underlying invert before exiting into the unsaturated zone below is determined by a common conceptual model that the physically localized immobile phases will primarily constrain that domain’s pH. However, these domain pH abstractions also include consideration of other environmental factors that link the environments between the domains (e.g., carbon dioxide partial pressure). There is one exception to the common conceptual model that is used for the case where seepage flow enters the waste package and the advected waste package effluent then enters the invert after traversing through the corrosion products domain. Under these conditions the invert pH is determined directly by the corrosion product domain (i.e., a direct link with no separate invert pH abstraction used).

1.1 WASTE FORM DOMAIN pH

The pH abstraction for the waste form domain (Cell 1) is based upon the local reactions with the solid phases, which includes not only the waste form(s) but also the contacting metal support structures, along with environmental conditions. Because of the inherently low pH buffering capacity of the incoming water (liquid-influx or vapor-influx), there is almost no dependence

upon the chemical range of incoming water composition (comparisons provided in SAR Figures 2.3.7-14, 2.3.7-15, and 2.3.7-17).

As relatively dilute seepage water flows (or water vapor condenses) into a waste package and contacts the waste form materials, its chemistry is determined by the dissolution of the waste form and waste package internal materials, secondary mineral precipitation and re-dissolution, and the in-drift carbon dioxide partial pressure. While the specific abstracted pH range also depends upon the waste package type and the ionic strength (which is dependent upon either the influx rate or waste package relative humidity), it is the set of well-defined chemical reactions that establish and constrain the abstracted range of pH within this domain, with the upper limit linearly dependent upon the log of the carbon dioxide partial pressure, and the lower limit buffered by the representative nickel-iron oxide mineral trevorite (NiFe_2O_4) (SNL 2007, Section 6.10.1[a]).

1.2 CORROSION PRODUCTS DOMAIN pH

The corrosion products domain, consisting of the degraded steel products (e.g., transportation, aging, and disposal canister and inner stainless steel vessel), is a physically separated flow path from the more stagnant fluid in the waste form domain, and as such is treated as being chemically distinct. The pH abstraction in the corrosion product domain (Cell 2) is founded upon the local reactions with the stationary corrosion products via competitive sorption reactions (the surface complexation model). However, the abstraction utilizes a sampling of potential waste form domain radionuclide-containing solutions as input fluids to derive its abstracted pH equation. As such, the abstraction contains an inherent relationship to the waste form chemical composition.

Conceptually, once a fluid packet begins transporting radionuclides out of the waste form domain, it must pass through the corrosion products domain where the corrosion products affect the fluid pH in isolation from the waste form. As the radionuclide flow enters the corrosion products domain, it does not carry a significant amount of dissolved solids from the waste form domain, and therefore has a limited capacity to self-buffer its pH. Compared with the bulk quantity of corrosion product solids with high-surface area that is acting as a porous chemical sorption-filter, the waste form fluid is readily buffered to the pH of the corrosion product surface-sorption sites. However, the waste form fluid is not determined by corrosion product composition and sorption reactions alone (SAR Section 2.3.7.5.3.1). The pH in the corrosion product domain also depends upon the drift-wide carbon dioxide partial pressure and an observed feedback from dissolved uranium concentration (due to its preferred sorption as a carbonate-complex species).

Therefore, although the corrosion products domain pH abstraction is distinct from that used in the waste form domain, both domain pH abstractions have a very similar dependence upon the partial pressure of carbon dioxide, and as both domains use the same in-drift gas pressure, a strong correlation exists between the models for pH in these two domains.

1.3 INVERT DOMAIN pH

The pH abstraction for the invert (Cell 3) is dependent upon whether or not there is advective flow through the waste package. For cases with advective flow through the waste package, as the waste package effluent leaves the corrosion product domain and enters the invert (flow path F₄ in SAR Figure 2.3.7-8), mixing will occur with the water that has dripped into the drift and has been diverted around the drip shield or waste package and imbibed into the invert (flow paths F₇, F₃, and F₅ in SAR Figure 2.3.7-8).

Where seepage flow occurs and results in advective flow through the waste package, the pH of the effluent that enters and flows through the invert after traversing through the corrosion products domain is directly represented by the corrosion product domain pH (i.e., a direct relationship exists with no separate invert abstraction). The crushed tuff invert, being composed of the relatively inert host rock material and having a submeter thickness, does not have a strong or rapid buffering capacity to overcome the more concentrated fluid being released from the waste package.

For breached waste packages not exposed to water influx conditions (i.e., there is no seepage or condensation at that location, or the drip shield is still diverting seepage flow), only vapor influx occurs into the waste package and only diffusive release of radionuclides to the invert occurs. With this limited diffusion-only release from the corrosion products domain, the fluid properties of the invert (e.g., ionic strength and pH) are determined by the in-drift seepage evaporation abstraction. That abstraction is based upon host-rock pore-water compositions that are modeled at the local repository conditions considering temperature, relative humidity, and the carbon dioxide partial pressure.

1.4 SUMMARY OF DOMAIN pH RELATIONS

The pH abstractions in the three EBS radionuclide transport domains are appropriately integrated taking into account the physical differences within the individual domains. The common conceptual model is that the local pH is primarily determined by buffering reactions with the dominant solid in the given domain (waste form degradation products, corrosion products, or tuff). The exception is the case of advection through the waste package where it is assumed that the local pH in the invert will be dominated by the waste package effluent and its associated equilibrium with the corrosion products. Important interrelationships include the following:

- All domains consider the same in-drift partial pressure of carbon dioxide and have their pH values correlated through that pressure
- The corrosion products domain pH abstraction is based upon a sampling of potential waste form fluid compositions
- The invert domain directly switches to the abstracted pH results from the corrosion products domain when there is liquid-influx/advective release from the waste package.

As a result of the integrated relationships between the pH abstractions of the three EBS radionuclide transport domains, the EBS release rates are appropriately estimated using the pH abstractions of those EBS domains.

2. COMMITMENTS TO NRC

None.

3. DESCRIPTION OF PROPOSED LA CHANGE

None.

4. REFERENCES

SNL (Sandia National Laboratories) 2007. *In-Package Chemistry Abstraction*.
ANL-EBS-MD-000037 REV 04 ADD 01. Las Vegas, Nevada: Sandia National Laboratories.
ACC: DOC.20070816.0004; DOC.20051130.0007; LLR.20080325.0276.

RAI: Volume 3, Chapter 2.2.1.3.4, First Set, Number 9:

Justify the use of high-temperature Pu solubility experimental data in fitting the adjusted-Eh Pu solubility abstraction as it applies to all repository thermal conditions.

Basis: The Eh-pH equation used in the adjusted-Eh abstraction for the Pu concentration limit was selected so that the resulting curve of Pu concentration versus pH passes through a set of published Pu solubility experimental results (SAR Figure 2.3.7-37). Some of the data used in SAR Figure 2.3.7-37, however, were obtained at temperatures of 60° and 90° C (Nitsche, et al., 1993, 1994; Efurd, et al. 1998), which are higher than long-term conditions in the waste package. For Pu, higher temperatures result in lower solubility limits (SNL, 2007a, Section 6.3.3.3) and therefore lower release rates. The high-temperature data, therefore, may inappropriately skew the range of experimental data to lower values. Without the 60° and 90° C results, nearly every data point in SAR Figure 2.3.7-37 falls above the mean curve that was apparently fit through the data. The requested information is needed to verify compliance with 10 CFR 63.21(c)(11)-(15) and 63.114(a) and (b).

1. RESPONSE

The high-temperature plutonium solubility experimental data were not used to fit the adjusted-Eh plutonium solubility abstraction. The experimental data that were used to fit the adjusted-Eh plutonium solubility model were taken at 22°C by Rai (1984). The 60°C and 90°C temperature data points from work by Nitsche et al. (1993 and 1994) and Efurd et al. (1998) were not used to create the adjusted-Eh solubility model, because they are not relevant to long-term conditions in the waste package and they represent lower solubilities than data at ambient temperature. As discussed in SAR Section 2.3.7.13.3, the solubility modeling of actinides was at 25°C. Therefore, the results modeled with the adjusted-Eh plutonium solubility model predict release rates relevant to long-term conditions in the waste package.

As requested by the NRC staff at the clarification meeting on April 1, 2009, additional information regarding the establishment of the Eh-pH relation for the adjusted-Eh solubility model is provided. The adjusted-Eh solubility model was developed based on examination of experimental data and repository-relevant conditions. As discussed in SAR Section 2.3.7.10.3.1, plutonium solubility calculated at an atmospheric fO_2 of 0.2 bar is significantly above the measured solubility from experiments (Efurd et al. 1998; Nitsche et al. 1993 and 1994; Rai 1984; Rai et al. 2001). Furthermore, the predicted plutonium species using atmospheric fO_2 of 0.2 to calculate Eh were not consistent with these experimental data. For example, the dominant plutonium species is Pu(V) in experiments conducted by others for pH from 3.5 to 5 (Rai 1984) and for pH from 6 to 8.5 (Nitsche et al. 1993 and 1994). In natural waters, plutonium(V) is observed to be the dominant dissolved species (Choppin et al. 1986). However, as shown in *Dissolved Concentration Limits of Elements with Radioactive Isotopes* (SNL 2007, Figure V-5), the oxidation state distribution in the solubility modeling results using $fO_2 = 0.2$ bars, shows that Pu(VI) is the dominant species over the entire pH range modeled. Therefore, the plutonium

solubility model using atmospheric fO_2 of 0.2 bars does not adequately represent plutonium behavior in aqueous systems because the solubility model (due to differing oxidation states of plutonium) is sensitive to redox potential. The discrepancy between the plutonium solubility model prediction results using atmospheric fO_2 and solubility experiments, as well as plutonium species observed in natural waters, led to the development of the adjusted-Eh solubility model.

As discussed in *Dissolved Concentration Limits of Elements with Radioactive Isotopes* (SNL 2007), further refinement of the solubility model was obtained by incorporating experimental data results from natural waters. Baas Becking et al. (1960) analyzed 6,200 Eh and pH measurements in natural waters and found that for pH between 3.2 and 12.6 there is an upper boundary for Eh-pH conditions that is shown in equation 1 (Baas Becking et al. 1960). Equation 1 is a more realistic boundary of redox conditions in natural waters that are in contact with the atmosphere than using atmospheric oxygen fugacity alone (Krauskopf and Bird 1995).

$$\text{Eh} = 1.04 - 0.0592 \text{ pH} \quad (\text{Eq. 1})$$

Comparison of predicted plutonium solubility, using Eh calculated from Equation 1, and experimental data on plutonium solubility is shown in Figure 1. While most of the measured plutonium solubility data fall within the uncertainty range of the model, the mean modeled plutonium concentration is below most of the experimental results taken at ambient temperature. Furthermore, some of the experimental data fall above the upper bound set by the Eh solubility model when Equation 1 is used. Therefore, the adjusted-Eh solubility model was developed because the modeled plutonium solubility results using Eh calculated from Equation 1 are lower than the experimental solubility results.

As discussed in SAR Section 2.3.7.10.3.1, the adjusted-Eh solubility model uses Eh calculated as shown in Equation 2. This adjusted-Eh equation was derived by adding 0.06 volts to the calculated Eh value given in Equation 1 for pH values between 3.2 and 12. The rationale for adding 0.06 volts is that measured Eh data from Rai (1984) are about 0.06 volts higher than values obtained from Equation 1. Thus, the Rai (1984) data that are measured at 22°C were used to fit the adjusted-Eh plutonium solubility model.

$$\text{Eh} = 1.10 - 0.0592 \text{ pH} \quad (\text{Eq. 2})$$

Using the adjusted-Eh solubility model, most of the data points from the solubility experiments fall within the uncertainty range of the adjusted-Eh solubility model, as shown in Figure 2. Importantly, none of the data points are above the upper bound of the adjusted-Eh solubility model. As requested by the NRC, Figure 2 (from SAR Figure 2.3.7-37) has been created without the high-temperature data. Note, there is no change to the modeled plutonium solubility results due to the fact that the high-temperature data were not used in the development of the adjusted-Eh solubility model.

Plausible explanations for the higher apparent plutonium solubility in experimental data include colloid formation and high ionic strengths. For example, measured aqueous plutonium concentrations are not only true dissolved plutonium, but contain plutonium colloids or polymers that are not excluded by the filter size. Kim and Kanellakopulos (1989) reported that a large

percent of plutonium was in plutonium(IV) colloid form even though the filter size was as small as 1 nm. Experimental solutions used by Rai et al. (2001) had higher ionic strengths than that modeled, which also yields a higher solubility.

In summary, the development of the adjusted-Eh solubility model is based upon experimental Eh data on natural waters, plutonium solubility, and speciation. The high-temperature plutonium solubility experimental data presented in SAR Figure 2.3.7-37 were not used for model development. Only data at 22°C reported by Rai (1984) were used to fit the adjusted-Eh solubility model. Thus, the adjusted-Eh solubility model appropriately represents the range of experimental data consistent with the long-term conditions in the waste package.

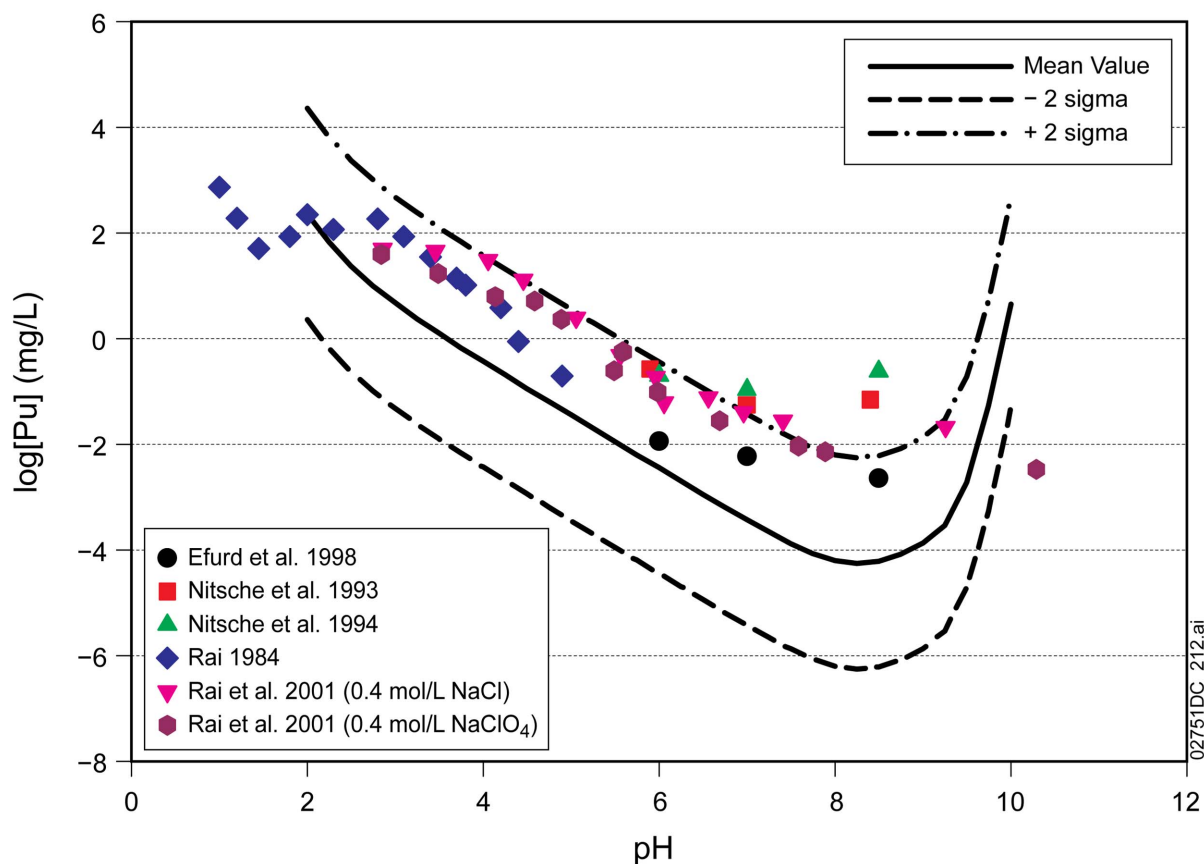
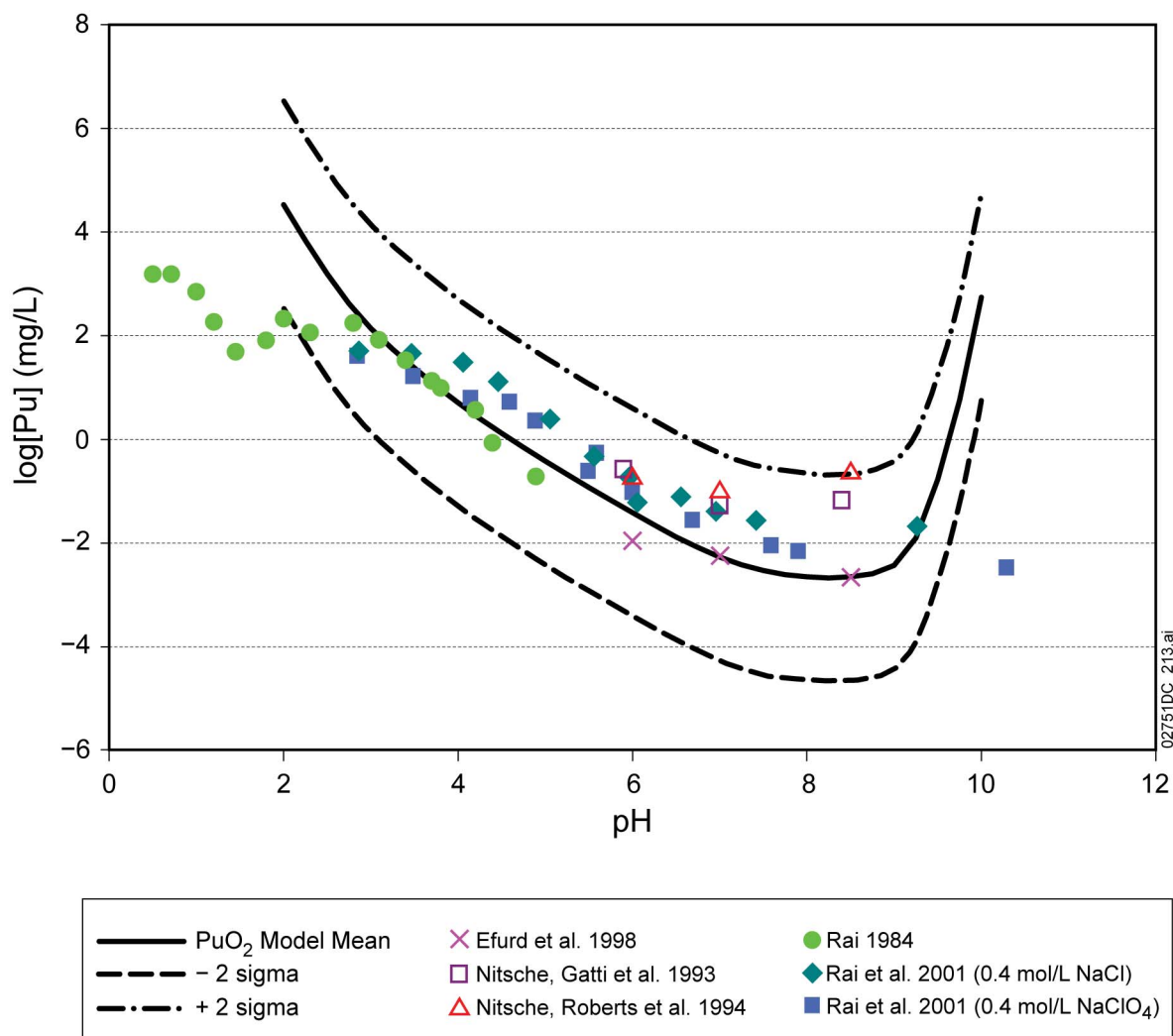


Figure 1 Comparison of Ambient Temperature Experimental Data to the Predicted Plutonium-Solubility Model Using Equation 1 to Calculate Eh



NOTE: This figure is the same as SAR Figure 2.3.7-37 but without the high-temperature experimental data.

Figure 2 Comparison of Ambient Temperature Experimental Data to the Predicted Plutonium-Solubility Model Using the Adjusted-Eh Solubility Model, Equation 2 to Calculate Eh

2. COMMITMENTS TO NRC

None.

3. DESCRIPTION OF PROPOSED LA CHANGE

None.

4. REFERENCES

Baas Becking, L.G.M.; Kaplan, I.R.; and Moore, D. 1960. "Limits of the Natural Environment in Terms of ph and Oxidation-Reduction Potentials." *Journal of Geology*, 68, (3), 243-284. Chicago, Illinois: University of Chicago Press.

Choppin, G.R.; Roberts, R.A.; and Morse, J.W. 1986. "Effects of Humic Substances on Plutonium Speciation in Marine Systems." *Organic Marine Geochemistry*. Sohn, M.L., ed. ACS Symposium Series 305, 382-388. Washington, D.C.: American Chemical Society.

Efurd, D.W.; Runde, W.; Banar, J.C.; Janecky, D.R.; Kaszuba, J.P.; Palmer, P.D.; Roensch, F.R.; and Tait, C.D. 1998. "Neptunium and Plutonium Solubilities in a Yucca Mountain Groundwater." *Environmental Science & Technology*, 32, (24), 3893-3900. Easton, Pennsylvania: American Chemical Society.

Kim J.I. and Kanellakopulos B. 1989. "Solubility Products of Plutonium(IV) Oxide and Hydroxide." *Radiochimica Acta*, 48, 145-150. Munich, Germany: R. Oldenbourg Verlag.

Krauskopf, K.B. and Bird, D.K. 1995. *Introduction to Geochemistry*. 3rd Edition. New York, New York: McGraw-Hill.

Nitsche, H.; Gatti, R.C.; et al., 1993. *Measured Solubilities and Speciations of Neptunium, Plutonium, and Americium in a Typical Groundwater (J-13) from the Yucca Mountain Region*. Los Alamos, New Mexico: Los Alamos National Laboratory. ACC: NNA.19930507.0136.

Nitsche, H.; Roberts, K.; et al., 1994. *Measured Solubilities and Speciations from Oversaturation Experiments of Neptunium, Plutonium, and Americium in UE-25P #1 Well Water from the Yucca Mountain Region* Milestone Report 3329-WBS1.2.3.4.1.3.1. Los Alamos, New Mexico: Los Alamos National Laboratory. ACC: NNA.19931015.0073.

Rai D. 1984. "Solubility Product of Pu(IV) Hydrous Oxide and Equilibrium Constants of Pu (IV)/Pu (V), Pu (IV)/Pu (VI), and Pu (V)/Pu (VI) Couples." *Radiochimica Acta*, 35, 97-106. München, Germany: R. Oldenbourg Verlag.

Rai, D.; Moore, D.A.; Felmy, A.R.; Choppin, G.R.; and Moore, R.C. 2001. "Thermodynamics of the PuO_2^+ - Na^+ - OH^- - Cl^- - ClO_4^- - H_2O System: Use of NpO_2^+ Pitzer Parameters for PuO_2^+ ." *Radiochimica Acta*, 89, (8), 491-498. München, Germany: Oldenbourg Wissenschaftsverlag.

SNL (Sandia National Laboratories) 2007. *Dissolved Concentration Limits of Elements with Radioactive Isotopes*. ANL-WIS-MD-000010 REV 06. Las Vegas, Nevada: Sandia National Laboratories. ACC: DOC.20070918.0010.

RAI: Volume 3, Chapter 2.2.1.3.4, First Set, Number 10:

For the adjusted-Eh Pu solubility limit model, provide the basis for (i) the applicability of the oxidation-reduction conditions under which supporting Pu solubility data were obtained, and (ii) the applicability of Yucca Mountain region groundwaters and miniature waste package experiments in supporting the adjusted-Eh equation. Demonstrate that the adjusted-Eh abstraction does not result in underestimation of reasonable Pu concentration limits.

Basis: The adjusted-Eh Pu model is intended to apply to conditions inside a breached waste package that is likely to have access to atmospheric O₂ concentrations. The data to which the model was fitted included experimental Pu solubility experiments conducted in closed vessels originally under air (Rai, 1984; Rai, et al., 2001), but also experiments conducted in the absence of O₂ (Nitsche, et al., 1993, 1994; Efurd, et al. 1998) – counter to a implication on SAR page 2.3.7-55 that all experiments were “originally open to the air.” None of the experiments allowed free exchange with air, as would potentially be the case in a breached package as assumed in the model abstraction and which would facilitate increased release rates.

In addition, the Eh-pH conditions measured in all sets of experiments were well below the adjusted-Eh model line. It is not clear that the experimental conditions were all “comparable to the modeled conditions” (SNL, 2007a, p 6-57). Figure V-6 of SNL (2007a) shows that the adjusted-Eh model line lies above all Yucca Mountain groundwater measurements; these data, however, were obtained from the saturated zone and therefore may have limited applicability in the case of the interior of a breached waste package in the unsaturated zone. Appendix V of SNL (2007a) also argues that redox conditions inside miniature waste packages—as constrained by the formation of magnetite—in experiments by Zarrabi, et al. (2003) were well below the adjusted-Eh line. These experiments, however, also contained ferric oxyhydroxides that indicate more oxidizing conditions than the hematite-magnetite buffer. In addition, the Zarrabi, et al. (2003) experiments employed carbon steel, which is now excluded from CSNF waste packages. The requested information is needed to verify compliance with 10 CFR 63.21(c)(11)-(15) and 63.114(a), (b), and (g).

1. RESPONSE

1.1 INTRODUCTION

The cited experiments were conducted under conditions representative of open-to-air conditions, even though the experimental vessels were closed to air during the experiments, and thus the results are applicable for breached waste packages. The adjusted-Eh model does not rely on Yucca Mountain groundwater measurements, and the model does not rely on the data from the miniature waste package experiments discussed in Section V.4 of *Dissolved Concentration Limits of Elements with Radioactive Isotopes* (SNL 2007); thus, their applicability does not impact the validity of the adjusted-Eh model. The experiments used to support the adjusted-Eh plutonium solubility model were conducted under conditions representative of open-to-air conditions. The redox potential used to develop the model is bounding, and thus it does not result in underestimation of plutonium solubility.

1.1.1 Open-to-Air Conditions

Breached waste packages in the repository are assumed to have access to atmospheric O₂ concentration (hereafter referred to as open-to-air conditions), which has a partial pressure (P_{O_2}) of 0.21 bars.

Since plutonium solubility is very sensitive to small changes in redox conditions, it is necessary to examine open-to-air conditions closely in order to have a realistic plutonium solubility model to support the total system performance assessment (TSPA).

Redox potential (Eh), rather than P_{O_2} , is more commonly used to present redox conditions when redox reactions are of interest. For $P_{O_2} = 0.21$ bars, the equivalent Eh value for aqueous solutions is a function of pH:

$$Eh(V) = 1.22 - 0.0592 \text{ pH} \quad (\text{Eq. 1})$$

This is the theoretical upper boundary of the water stability field in an Eh-pH diagram.

Analyzing 6,200 Eh and pH measurements in natural waters, Baas Becking et al. (1960) found that for pH between 3.2 and 12.6, there is an empirical upper boundary for Eh-pH conditions in natural waters:

$$Eh(V) = 1.04 - 0.0592 \text{ pH} \quad (\text{Eq. 2})$$

No counter-example to this upper boundary has been reported for natural waters since it was reported nearly five decades ago. Therefore, for a redox-sensitive system, it is more appropriate to represent open-to-air conditions using Equation 2 rather than Equation 1.

The adjusted-Eh model uses Equation 3:

$$Eh(V) = 1.10 - 0.0592 pH \quad (\text{Eq. 3})$$

to calculate plutonium solubility, which is 60 mV higher than Equation 2 and results in higher plutonium solubilities than Equation 2, to ensure that the calculated plutonium solubility is bounding (SNL 2007). This treatment is consistent with the fact that “dissolved oxygen does not exert the potential expected if it is functioning at equilibrium” (Garrels and Christ 1990).

The distribution of plutonium species of different oxidation states largely depends on redox conditions. In general, higher redox potential results in a distribution dominated by high-valence plutonium species and higher plutonium solubility.

Measurements made for water samples from the Irish Sea, into which plutonium was released from a nearby reprocessing plant (Nelson and Lovett 1978), and measurements made for water samples from the Pacific Ocean (Nelson et al. 1984) revealed that, in those sea waters, dissolved plutonium exists mainly in high oxidation states (i.e., plutonium(V) and plutonium(VI)).

Other measurements made by Bondietti and Trabalka (1980) further demonstrate that plutonium(V) is the dominant valence in natural waters.

Choppin et al. (1986) reported their findings about plutonium species distribution in sea waters. They added plutonium as 100% plutonium(VI) into artificial sea water and natural sea water from the Gulf of Mexico; it was observed that plutonium(VI) was rapidly reduced to plutonium(V) and plutonium(IV). Plutonium(V) is the dominant plutonium species when no organics exist. When sea water has organics, plutonium(V) is further reduced to plutonium(IV) (Choppin et al. 1986).

These data demonstrate that under open-to-air conditions, plutonium(V) is the dominant plutonium species. Redox potentials in natural waters are not high enough to maintain plutonium(VI) as the dominant species.

In summary, under open-to-air conditions, Eh is lower than that given by Equation 1 and an empirical upper boundary for Eh is given by Equation 2. Moreover, under open-to-air conditions, plutonium(V) is the dominant species. These two facts can be related to each other; (i.e., under open-to-air conditions) redox conditions of aqueous systems are lower than the theoretical values so that plutonium is dominated by plutonium(V).

1.2 APPLICABILITY OF PLUTONIUM SOLUBILITY EXPERIMENTS

Results from five sets of plutonium solubility experiments were used to develop the adjusted-Eh plutonium solubility model. These experiments were reported by Rai et al. (2001), Rai (1984), Nitsche et al. (1993, 1994), and Efurd et al. (1998).

Experiments reported by Rai et al. (2001) are intended to determine plutonium solubility in air-equilibrated solutions. Although the centrifuge tubes were tightly capped during

experiments, they were not totally filled with experimental solutions. Each centrifuge tube contained about 20 ml air (Rai et al. 2001). Estimation of O₂ consumption by conceivable oxidizing reactions occurring in the tube demonstrated that only a few percent of O₂ in the gaseous phase may be consumed (see Appendix A of this response). Thus, this amount of air was enough to maintain open-to-air conditions. Furthermore, these tubes were periodically opened during the experiments to make measurements, which also helped to maintain open-to-air conditions. Therefore, there is no reason to conclude that the experiments were not open-to-air.

Experiments reported by Rai (1984) were conducted for conditions similar to those reported by Rai et al. (2001), although experimental procedures described in the former were not described in as much detail as in the latter. Nonetheless, similar results were produced. Thus, there is also no reason to conclude that experiments reported by Rai (1984) were not open-to-air.

There is corroborative evidence supporting that those experiments were conducted under conditions representative of open-to-air conditions.

First, the Eh-pH relation measured in those experiments follows Equation 3 for pH between 2 and 3.8, which is 60 mV higher than Equation 2, the empirical upper boundary of redox potential in natural water (of Chen and Pearson 2008, Figure 6). Although it is noticeable that, for pH > 4.25, the measured Eh is lower than the values given by Equation 3, this is attributed by the author (Rai et al. 2001) to poor poisoning of the systems. This explanation is supported by the fact that the modeled plutonium solubilities using Equation 3 match experimental results very well for the range of pH of interest, including pH > 4.25.

Second, the observation that plutonium(V) is the dominant plutonium species in those experiments (Rai 1984, Table 3) for pH > 3 is consistent with the observations for natural waters. The consistent results further support that the experiments were conducted under conditions representative of open-to-air conditions.

The three sets of experiments reported by Nitsche et al. (1993, 1994) and Efurd et al. (1998) followed similar procedures. Although those experiments were closed to air, the solution was originally open to air. Again, the fact that in those experiments plutonium(V) is the dominant plutonium species (Table II in Nitsche et al. 1993; Table II in Nitsche et al. 1994) is consistent with the observations for natural waters and from Rai's experiments (Rai et al. 2001; Rai 1984). Thus, the conditions for those experiments were representative of open-to-air conditions as well.

In summary, all five sets of plutonium solubility experiments were conducted under conditions representative to open-to-air conditions, and thus the results are applicable to breached waste packages.

1.3 APPLICABILITY OF REDOX CONDITIONS OF YUCCA MOUNTAIN REGION GROUNDWATERS AND WITHIN BREACHED WASTE PACKAGES

SAR Figure 2.3.7-36 shows that all Eh-pH measurements for Yucca Mountain region groundwater are below the adjusted-Eh equation. This figure was presented as corroborative evidence for the adjusted-Eh model, in that from it one could infer that the adjusted-Eh model is

conservative. The development of the adjusted-Eh model does not directly rely on these measurements. Thus, the applicability of those groundwater measurements to breached waste packages is not discussed in this response.

Similarly, the discussion in Section V.4 of *Dissolved Concentration Limits of Elements with Radioactive Isotopes* (SNL 2007) is meant to show that redox conditions within breached waste packages may be lower than those given by Equation 3; thus, the adjusted-Eh model is conservative. The arguments presented in Section V.4 of *Dissolved Concentration Limits of Elements with Radioactive Isotopes* (SNL 2007) were not used to develop the model.

Solubility, as it is applied in the TSPA model, is a bounding property. By using Equation 3 to calculate plutonium solubility, the bounding requirement on redox potential is satisfied, because Equation 3 is even higher than the empirical upper boundary of Eh represented by Equation 2. The relation between Equation 3 and redox conditions of Yucca Mountain groundwater and within breached waste packages determines whether this solubility model is conservatively bounding or realistically bounding, but it has no bearing on the bounding feature of the adjusted-Eh model. In other words, whether the redox conditions of Yucca Mountain groundwaters and of miniature waste packages are applicable to breached waste packages located in the unsaturated zone has no impact on the validity of the adjusted-Eh model.

1.4 CONCLUSION – THE ADJUSTED-EH PLUTONIUM SOLUBILITY MODEL IS BOUNDING

The experiments used to support the adjusted-Eh model were conducted under open-to-air conditions and their results are applicable to breached waste packages. Equation 3, which was used to develop the model, is an upper boundary of redox potential that can occur in natural waters and within breached waste packages. As a result, the adjusted-Eh model, with uncertainties accounted for, provides a bounding estimate on plutonium solubility. Therefore, it does not result in underestimation of plutonium solubility.

2. COMMITMENTS TO NRC

None.

3. DESCRIPTION OF PROPOSED LA CHANGE

None.

4. REFERENCES

Baas Becking, L.G.M.; Kaplan, I.R.; and Moore, D. 1960. "Limits of the Natural Environment in Terms of pH and Oxidation-Reduction Potentials." *Journal of Geology*, 68, 243-284.

Bondietti, E.A.; and Trabalka, J.R. 1980. "Evidence for Plutonium/V/ in an Alkaline, Freshwater Pond." *Radiochemical and Radioanalytical Letters*, 42 (3), 169-176.

Chen, Y.; Pearson, F.J. 2008. "Modeling Plutonium Solubility for Yucca Mountain Performance Assessment." *Radiochimica Acta*, 96, 521-526.

Choppin, G.R.; Roberts, R.A.; and Morse, J.W. 1986. "Effects of Humic Substances on Plutonium Speciation in Marine Systems." *Organic Marine Geochemistry*. Sohn, M.L., ed. ACS Symposium Series 305. Pages 382-388. Washington, D.C.: American Chemical Society.

Efurd, D.W.; Runde, W.; Banar, J.C.; Janecky, D.R.; Kaszuba, J.P.; Palmer, P.D.; Roensch, F.R.; and Tait, C.D. 1998. "Neptunium and Plutonium Solubilities in a Yucca Mountain Groundwater." *Environmental Science & Technology*, 32, (24), 3893-3900. Easton, Pennsylvania: American Chemical Society.

Garrels, R.M. and Christ, C.L. 1990. *Solutions, Minerals, and Equilibria*. Boston, Massachusetts: Jones and Bartlett Publishers.

Langmuir, D. 1997. *Aqueous Environmental Geochemistry*. Upper Saddle River, New Jersey: Prentice Hall.

Nelson, D.M.; Lovett, M.B. 1978. "Oxidation State of Plutonium in the Irish Sea." *Nature*, 276, (5688), 599-601.

Nelson, D.M.; Carey, A.E.; Bowen, V.T. 1984. "Plutonium Oxidation State Distributions in the Pacific Ocean During 1980-1981." *Earth and Planetary Science Letters*, 68, 422-430.

Nitsche, H.; Gatti, R.C.; Standifer, E.M.; Lee, S.C.; Muller, A.; Prussin, T.; Deinhammer, R.S.; Maurer, H.; Becroft, K.; Leung, S.; and Carpenter, S.A. 1993. *Measured Solubilities and Speciations of Neptunium, Plutonium, and Americium in Typical Groundwater (J-13) from the Yucca Mountain Region*. LA-12562-MS. Los Alamos, New Mexico: Los Alamos National Laboratory. ACC: MOL.19950621.0265.

Nitsche, H.; Roberts, K.; Prussin, T.; Muller, A.; Becroft, K.; Keeney, D.; Carpenter, S.A.; and Gatti, R.C. 1994. *Measured Solubilities and Speciations from Oversaturation Experiments of Neptunium, Plutonium, and Americium in UE-25P #1 Well Water from the Yucca Mountain Region Milestone Report 3329-WBS1.2.3.4.1.3.1*. LA-12563-MS. Los Alamos, New Mexico: Los Alamos National Laboratory.

Rai, D. 1984. "Solubility Product of Pu(IV) Hydrous Oxide and Equilibrium Constants of Pu (IV)/Pu (V), Pu (IV)/Pu (VI), and Pu (V)/Pu (VI) Couples." *Radiochimica Acta*, 35, 97-106. München, Germany: R. Oldenbourg Verlag.

Rai, D.; Moore, D.A.; Felmy, A.R.; Choppin, G.R.; and Moore, R.C. 2001. "Thermodynamics of the PuO_2^+ - Na^+ - OH^- - ClO_4^- - H_2O system: use of NpO_2^+ Pitzer parameters for PuO_2^+ ." *Radiochimica Acta*, 89, ([8]), 491-498. München, Germany: Oldenbourg Wissenschaftsverlag.

SNL (Sandia National Laboratories) 2007. *Dissolved Concentration Limits of Elements with Radioactive Isotopes*. ANL-WIS-MD-000010 REV 06. Las Vegas, Nevada: Sandia National Laboratory. ACC: DOC.20070918.0010.

APPENDIX A

POTENTIAL O₂ CONSUMPTION IN PLUTONIUM SOLUBILITY EXPERIMENTS

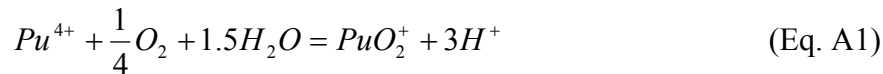
This appendix provides an estimate for the potential consumption of O₂ by reactions for converting Pu(IV) to Pu(V) and Pu(VI) in those Pu solubility experiments by Rai et al. (2001) and assesses its potential effects on the partial pressure of O₂ in the system.

In the centrifuge tubes, O₂ exists in two forms – in air that fills the void space and is dissolved in the solution. The void space is 20 ml (the volume of those centrifuge tubes was 50 ml, and the volume of experimental solution was 30 ml) (Rai et al. 2001). Assuming room temperature (25°C) and partial pressure of O₂ at 0.21 bars (Langmuir 1997), the amount of O₂ in the gaseous phase is 0.169 mmol.

Two conceivable mechanisms may consume O₂ in the Pu solubility experiments conducted by Rai et al. (2001): (1) oxidizing Pu(IV) into Pu(V) and Pu(VI) aqueous species, as the starting Pu material in the experiments was in Pu(IV); and (2) converting PuO₂(am,hyd) to PuO_{2+x}. Although the existence of PuO_{2+x} is still a topic of scientific research (Haschke and Allen 2000; Neck et al. 2007), its presence is assumed in this analysis.

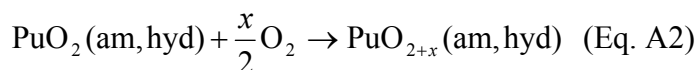
The Pu precipitation was made from 0.04 ml stock solution (Rai et al. 2001), which contains 0.0473 mmol of plutonium.

Oxidizing Pu(IV) aqueous species to Pu(V) species consumes O₂:



However, the maximum Pu solubility measured for 0.403 NaCl solution and 0.408 NaClO₄ solution is about 0.2 mmol/kg (Rai et al. 2001, Tables A1 and A2). Thus, for 30 ml solution, at most 0.006 mmol out of 0.0473 mmol Pu was in solution, which can consume at most 0.0015 mmol of O₂. That is less than 1% of O₂ in a centrifuge tube. In the above calculation, only oxidizing reactions converting plutonium(IV) to plutonium(V) aqueous species were considered. Including oxidizing reactions converting plutonium(IV) to plutonium(VI) aqueous species would result in higher O₂ consumption. However, because plutonium(VI) species is minor compared with plutonium(V) species, including it would not change the number significantly.

The reaction for converting PuO₂(am,hyd) to PuO_{2+x}(am,hyd) can be written as (Neck et al. 2007):



Neck et al. (2007) estimated that x has a maximum value of 0.25. Assuming all PuO_2 precipitation is available to be converted to PuO_{2+x} , then, in each centrifuge tube, the above reaction consumes $0.0473 \times 0.125 = 0.0059$ mmol of O_2 , which is about 3.5% of O_2 in the gaseous phase.

Therefore, O_2 consumption by converting plutonium(IV) solids to solids of mixture of plutonium(IV) and plutonium(V) is just a few percent of O_2 contained in the centrifuge tubes.

Combining mechanisms (1) and (2), the total potential O_2 consumption is less than 5%. This estimation is conservative, because the amount of plutonium in solution is also accounted for in the calculation for solid phase conversion. The dissolved O_2 in solution is neglected, which also results in an overestimation in O_2 consumption. Moreover, the above calculations assume that the centrifuge tubes were closed to air for the whole duration of experiments, which, as discussed in Section 1.2, is not the case (Rai et al. 2001).

In summary, O_2 consumption by conceivable oxidizing reactions is at most a few percentage of O_2 contained in a centrifuge tube without considering additional air supplied when it was opened for measurements. Therefore, it is concluded that oxidizing reactions do not significantly alter the redox conditions of the system from open-to-air conditions.

References

- Haschke, J.M.; Allen, T.H.; and Morales, L.A. 2000. "Reaction of Plutonium Dioxide with Water: Formation and Properties of PuO_{2+x} ." *Science*, 287, (5451), 285-287. Washington, D.C.: American Association for the Advancement of Science.
- Neck, V; Altmaier, M.; and Fanghänel, Th. 2007. "Thermodynamic Data for Hydrous and Anhydrous $\text{PuO}_{2+x}(s)$." *Journal of Alloys and Compounds*, 444-445, 464-469.
- Rai, D.; Moore, D.A.; Felmy, A.R.; Choppin, G.R.; and Moore, R.C. 2001. "Thermodynamics of the $\text{PuO}_2^+ - \text{Na}^+ - \text{OH}^- - \text{Cl}^- - \text{ClO}_4^- - \text{H}_2\text{O}$ system: use of NpO_2^+ Pitzer parameters for PuO_2^+ ." *Radiochimica Acta*, 89, (8), 491-498. München, Germany: Oldenbourg Wissenschaftsverlag.

RAI: Volume 3, Chapter 2.2.1.3.4, First Set, Number 11:

Provide the basis for using the adjusted-Eh redox conditions in modeling $\text{NaNpO}_2\text{CO}_3$ solubility for the Np concentration limits abstraction. Provide justification that use of adjusted-Eh conditions for this Np solid phase will not unreasonably lead to underestimation of dissolved Np concentration.

Basis: According to SNL (2007a, page 6-67), the adjusted-Eh model was used to calculate $\text{NaNpO}_2\text{CO}_3$ solubilities that apply to the Np concentration limit abstraction at certain pH and CO_2 partial pressure conditions. The adjusted-Eh model was developed for the Pu abstraction by fitting Pu solubility models to Pu experimental data. Its applicability to the Np abstraction is not clear. As discussed in RAI 2.2.1.3.4-CL3, that the adjusted-Eh model is more oxidizing than Yucca Mountain groundwaters is not a sufficient basis for the model's applicability. The requested information is needed to verify compliance with 10 CFR 63.21(c)(11)-(15) and 63.114(a), (b), and (g).

1. RESPONSE

Because water in contact with the atmosphere will not reach Eh levels consistent with those for atmospheric oxygen, it is reasonable to lower the Eh of the system modeled. Corrosion of waste package materials and waste forms consumes oxygen, lowering redox conditions within waste packages to levels lower than that given by the empirical-Eh equation. This process will further reduce redox conditions within the package before the package is fully degraded.

1.1 ADJUSTED EH VERSUS EMPIRICAL EH

$\text{NaNpO}_2\text{CO}_3$ solubilities were calculated using the adjusted-Eh model. The Eh calculated by the adjusted-Eh equation used for $\text{NaNpO}_2\text{CO}_3$ is higher than the empirical upper boundary for Eh-pH conditions in various natural waters. The use of the adjusted-Eh equation to set redox conditions for $\text{NaNpO}_2\text{CO}_3$ is conservative.

Analysis of 6,200 Eh and pH measurements in natural waters shows that for pH values between 3.2 and 12.6 there is an upper boundary for Eh-pH conditions in natural waters (Baas Becking et al. 1960), that is:

$$\text{Eh}(\text{volt.}) = 1.04 - 0.0592\text{pH} \quad (\text{Eq. 1})$$

In these 6,200 samples, not one measurement exceeded the limit set by Equation 1. This equation is a more-realistic boundary of redox conditions in natural waters that are in contact with the atmosphere (Krauskopf and Bird 1995) than setting the Eh equal to equilibrium with atmospheric oxygen.

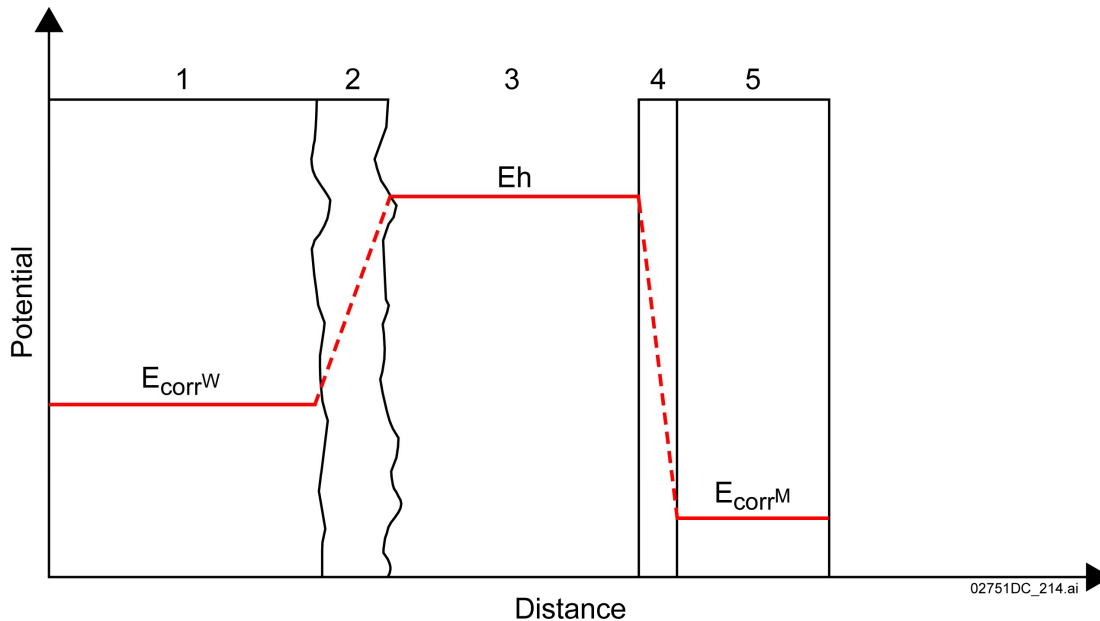
Measured Eh-pH values for waters obtained from wells at or near Yucca Mountain are presented in Figure V-6 of *Dissolved Concentration Limits of Elements with Radioactive Isotopes* (SNL 2007). Most of these measurements were made *in situ*, either downhole or using a

flow-through cell. Some samples are bailed samples. The *in situ* samples provide more accurate Eh measurements since equilibration with the atmosphere at the wellhead does not occur, as may happen in bailed samples taken in open containers. Figure V-6 of *Dissolved Concentration Limits of Elements with Radioactive Isotopes* (SNL 2007) shows that all the Eh–pH measurements made at Yucca Mountain are below the empirical boundary for Eh–pH conditions described by Equation 1, thus making the use of the adjusted-Eh model (Equation 2) (SNL 2007, Equation V-5) conservative.

$$Eh = 1.10 - 0.0592pH \quad (\text{Eq. 2})$$

1.2 WASTE PACKAGE CORROSION EFFECTS ON EH

Relevant neptunium reaction paths start in the waste forms and progress through the waste form alteration rind, the bulk solution, steel corrosion products, and corroding steel. A simple conceptualization of these paths is presented in Figure IV-2 of *Dissolved Concentration Limits of Elements with Radioactive Isotopes* (SNL 2007) and reproduced in Figure 1. This figure qualitatively illustrates the relevant potentials neptunium will “see” for reactions (as identified in five sections) occurring: (1) at the surface of the waste form, (2) in the waste form corrosion rind, (3) in the bulk solution, (4) in the corrosion product layer on steel surfaces, and (5) at the surface of a corroding steel.



NOTE: E_{corrW} = corrosion potential of the waste; Eh is the Eh of the bulk solution; E_{corrM} = corrosion potential of the waste package metals.

Figure 1. General Conceptualization for the Waste Form Corrosion and Metal Corrosion Reaction Paths

The Eh of the water in contact with waste package components will be strongly influenced by the UO₂ and steel. For example, in commercial spent nuclear fuel (SNF), the oxygen potential is less

than -400 kJ/mol (Dehaudt 2001, Section 5.2.6.5). Additionally, corrosion products from spent fuel and steel corrosion will limit the rates of oxygen transport within the waste packages.

No direct measurements of redox conditions within breached waste packages are available. Nonetheless, corrosion of waste package materials and waste forms consumes oxygen, thereby lowering redox conditions within waste packages as demonstrated through secondary iron mineralization in miniature waste packages. X-ray diffraction (XRD) analysis of corrosion products carried out of miniature waste packages by effluent documented that magnetite was commonly formed, along with lepidocrocite and goethite (Zarrabi et al. 2003, Table 10). Experiments with glass-walled miniature waste packages with carbon steel internals showed that as the duration or temperature of the experiments increased, the abundance of black magnetite increased. Formation of magnetite indicates that portions of the environment within the miniature waste package were below the Eh–pH line defined by the hematite and magnetite boundary line (Equation 3).

$$Eh \text{ (volt)} = 0.221 - 0.0592pH \quad (\text{Eq. 3})$$

The miniature waste package experiments commonly produced magnetite corrosion products, indicating that portions of the miniature waste package environment were reducing and not in equilibrium with atmospheric oxygen levels. The lower oxygen levels occurred despite the smaller size and surface area of the miniature waste packages. Therefore, these miniature waste package experiments support the hypothesis that a reducing environment would form within the waste package.

Breached waste packages within the repository will also not be totally open to air, and transport of oxygen gas into the waste package is limited by waste package cracks or holes that can be plugged by corrosion products of waste package materials and waste forms. This is supported by Zarrabi et al. (2003, Sections 4.1 and 5), where corrosion products within the miniature waste packages plugged holes in the waste packages, limiting transport of oxygen into the waste package and lowering redox conditions, thereby lowering neptunium solubility limits. Therefore, the use of the adjusted-Eh equation (Equation 2) for $\text{NaNpO}_2\text{CO}_3$ is conservative.

1.3 SUMMARY

The Eh calculated by the adjusted-Eh equation used for $\text{NaNpO}_2\text{CO}_3$ is higher than the empirical upper boundary for Eh–pH conditions in various natural waters (including measured Yucca Mountain waters). Additionally, corrosion of waste package materials and waste forms consumes oxygen, lowering redox conditions within waste packages to levels lower than that given by the empirical-Eh equation. Therefore, the use of the adjusted-Eh equation (Equation 2) to set redox conditions for $\text{NaNpO}_2\text{CO}_3$ is conservative and will not lead to underestimation of dissolved neptunium concentration.

2. COMMITMENTS TO NRC

None.

3. DESCRIPTION OF PROPOSED LA CHANGE

None.

4. REFERENCES

Baas Becking, L.G.M.; Kaplan, I.R.; and Moore, D. 1960. "Limits of the Natural Environment in Terms of pH and Oxidation-Reduction Potentials." *Journal of Geology*, 68, (3), 243-284. Chicago, Illinois: University of Chicago Press.

Dehaudt, P. 2001. "State of the Art of the Oxidation of Spent Nuclear Fuel." Section 7.2 of *Synthesis on the Long Term Behavior of the Spent Nuclear Fuel*. Poinsot, C., ed. CEA-R 5958(E). Volume II. Paris, France: Commissariat à l'Énergie Atomique.

Krauskopf, K.B. and Bird, D.K. 1995. *Introduction to Geochemistry*. 3rd Edition. New York, New York: McGraw-Hill.

SNL (Sandia National Laboratories) 2007. *Dissolved Concentration Limits of Elements with Radioactive Isotopes*. ANL-WIS-MD-000010 REV 06. Las Vegas, Nevada: Sandia National Laboratory. ACC: DOC.20070918.0010.

Zarrabi, K.; McMillan, S.; Elkonz, S.; and Cizdziel, J. 2003. *Corrosion and Mass Transport Processes in Carbon Steel Miniature Waste Packages*. Document TR-03-003, Rev. 0. Task 34. Las Vegas, Nevada: University of Nevada, Las Vegas.

RAI: Volume 3, Chapter 2.2.1.3.4, First Set, Number 12:

Clarify whether or not Np incorporation into uranyl minerals is included in any aspects of the Np concentration limits conceptual model. Provide justification that addresses the inconsistencies between the conceptual and alternative conceptual models described in the basis below.

Basis: As discussed in Appendix IV of SNL (2007a), DOE concluded that an Np concentration limit model that included incorporation into uranyl minerals did not have sufficient basis for inclusion in the base case. On page IV-6 of that same appendix, however, DOE relies on the conceptual model of Np co-precipitation in uranyl minerals to help support the use of an NpO_2 solubility model for CDSP packages in the nominal scenario and CSNF packages in the igneous intrusion scenario. This reliance on Np incorporation appears to be at odds with DOE's rejection of the alternative conceptual model. The requested information is needed to verify compliance with 10 CFR 63.21(c)(9), (11)-(15) and 63.114(b), (c), and (g).

1. RESPONSE

As indicated in *Dissolved Concentration Limits of Elements with Radioactive Isotopes* (SNL 2007, Section 6.6.3.1, Table 8-1, and Appendix IV), NpO_2 is used as the solubility-controlling phase in the waste package when there is a reductant, such as fuel or steel, present and Np_2O_5 is used as the primary solubility-controlling phase inside the waste package when all reducing materials are fully corroded. For the invert, the Np_2O_5 solubility model is always applied. A model of neptunium-containing uranyl phases has not been applied to the base case pure-phase neptunium solubility models supporting the total system performance assessment (TSPA).

Appendix IV of *Dissolved Concentration Limits of Elements with Radioactive Isotopes* (SNL 2007, p. IV-6) indicates that for commercial spent nuclear fuel (SNF) waste packages after an igneous event, and for codisposal waste packages in the nominal, igneous intrusion, and seismic scenarios, it is reasonable that there will be some co-precipitation of neptunium with uranyl phases. However, experimental data have not shown that a neptunium-incorporated uranyl phase can act as the solubility-controlling phase for neptunium. Although neptunium has been found to incorporate with some uranyl phases under laboratory conditions, observations of uranyl minerals in nature show that these solids do not contain high levels of impurities (SNL 2007, Section IV.3).

In summary, as described in *Dissolved Concentration Limits of Elements with Radioactive Isotopes* (SNL 2007, Appendix IV), when fuel or steel are still present within the waste package, NpO_2 is appropriately used as the solubility controlling phase. Although the phenomenon of neptunium incorporation into uranyl phases exists, amounts will be limited. Therefore, even though Np-uranyl solid solution phases may be present in codisposal waste packages or in commercial SNF waste packages after an igneous event, the continued presence of steel causes NpO_2 to remain as the primary neptunium solubility-controlling phase within the waste package.

ENCLOSURE 11

Response Tracking Number: 00261-00-00

RAI: 3.2.2.1.3.4-012

For this reason, neptunium incorporation into uranyl phases is not included in the neptunium solubility model used in the TSPA-LA.

2. COMMITMENTS TO NRC

None.

3. DESCRIPTION OF PROPOSED LA CHANGE

None.

4. REFERENCES

SNL (Sandia National Laboratories) 2007. *Dissolved Concentration Limits of Elements with Radioactive Isotopes*. ANL-WIS-MD-000010 REV 06. Las Vegas, Nevada: Sandia National Laboratory. ACC: DOC.20070918.0010.

RAI: Volume 3, Chapter 2.2.1.3.4, First Set, Number 13:

Compare the Np concentration limit abstractions against available laboratory data on Np pure-phase solubility limits. Provide justification that these data are either not applicable or support the adopted abstraction.

Basis: In developing and validating the Np concentration limits abstraction, DOE did not refer to laboratory measurements of Np concentrations in pure-phase solubility experiments (e.g., summary by Neck 2006), including data obtained by the Yucca Mountain Project (Nitsche et al., 1993, 1994; Efurd et al., 1998). At a given pH, the Np concentrations measured in these studies are 0.5 to 3 log units higher than the higher-Np Np_2O_5 DOE abstraction curve (SAR Figure 2.3.7-39). A higher Np concentration limit could result in higher Np release rates from the EBS. Neither the SAR nor the supporting AMR (SNL 2007) discussed these concentration results. Appendix IV of SNL (2007) does discuss the Np solid phase identifications in Nitsche et al. (1993, 1994) and Efurd et al. (1998) and argues that the solids are not representative of long-term repository conditions. The appendix (SNL 2007, page IV-15) also compares the Efurd et al. (1998) solubility constant with the abstraction value for Np_2O_5 and argues that the Efurd et al. (1998) value, though within the abstraction uncertainty bounds, is too high because it reflects hydrated Np_2O_5 . However, DOE has not transparently described available solubility data, including project data, that are relevant to the Np abstraction and has not evaluated whether the data are suitable for supporting the model abstraction. The requested information is needed to verify compliance with 10 CFR 63.21(c)(11)-(15) and 63.114(b) and (g).

1. RESPONSE

This RAI identifies four references (Efurd et al. 1998; Nitsche et al. 1993 and 1994; Neck 2006) that contain pure-phase neptunium solubility measurements that were not specifically compared to the concentrations in the Np_2O_5 model abstraction used in the total system performance assessment (TSPA). The referenced experimental data are plotted along with the Np_2O_5 model abstraction, which is used in the TSPA when all the fuel and steel within the waste package are fully oxidized and within the invert where oxidizing conditions are considered likely. For each reference, the measured concentrations observed in the experiments are either not applicable to Yucca Mountain due to the formation of metastable phases or are within the error bounds of the model abstraction used in the TSPA.

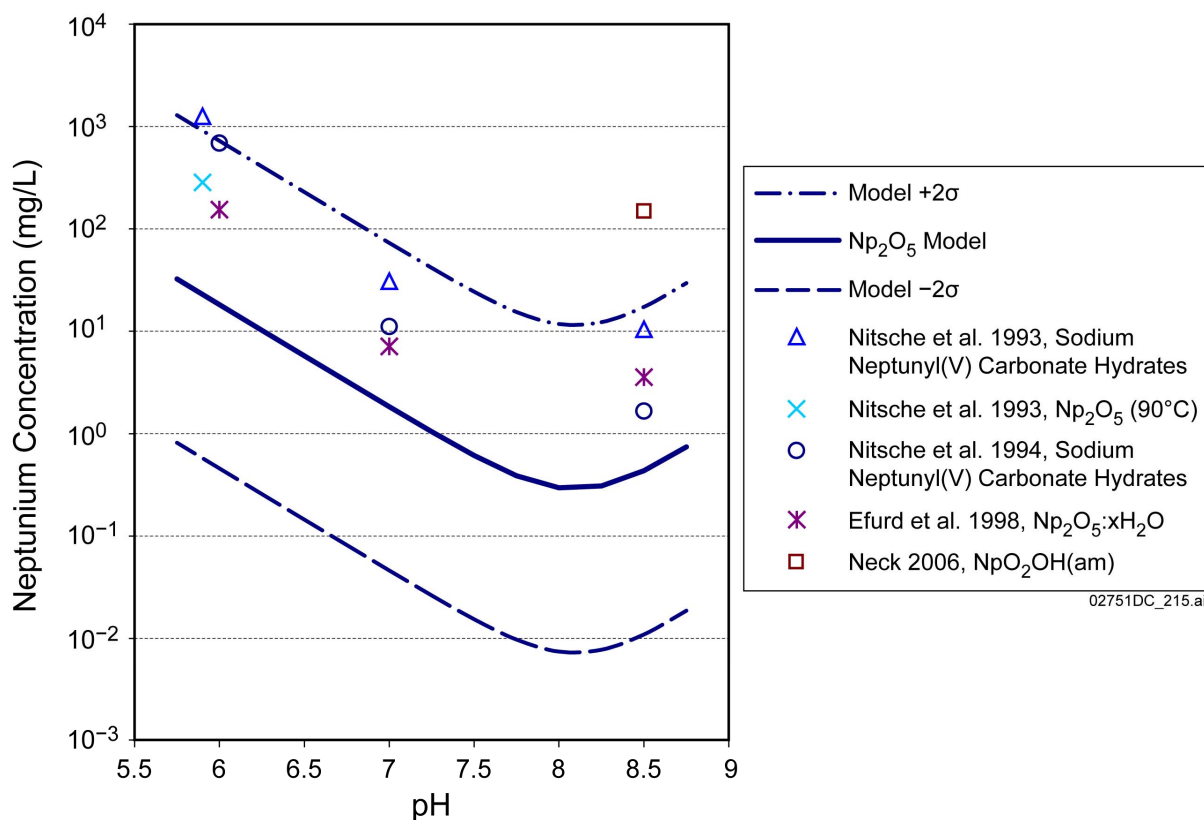
The pure-phase neptunium concentrations measured by Efurd et al. (1998) were not compared to the Np_2O_5 concentration limit abstraction in *Dissolved Concentration Limits of Elements with Radioactive Isotopes* (SNL 2007) because the solids that formed in those experiments were metastable phases ($\text{Np}_2\text{O}_5:x\text{H}_2\text{O}$) that would age over a period of less than 100 years at ambient temperature into the more stable anhydrous Np_2O_5 (SNL 2007, p. IV-15). Conversion to the more stable anhydrous Np_2O_5 , as noted by the higher crystallinity content in the experiments conducted at 90°C, further supports the selection of anhydrous Np_2O_5 as the controlling phase. Efurd et al. (1998) performed neptunium solubility experiments from over- and undersaturation

with respect to the $\text{Np}_2\text{O}_5:x\text{H}_2\text{O}$ phase. The neptunium concentrations measured by Efurd et al. (1998) are plotted in Figure 1 for comparison purposes, along with the concentrations calculated for the more thermodynamically stable anhydrous solid (Np_2O_5) used in the TSPA.

The pure-phase concentrations measured by Nitsche et al. (1993 and 1994) are not used in *Dissolved Concentration Limits of Elements with Radioactive Isotopes* (SNL 2007) for model development because the solids observed at 25°C and 60°C (sodium neptunyl(V) carbonate hydrates) were found to be stable only for waters with high sodium concentrations (>0.05 molar), like those solutions used in their experiments, and at neutral pH values (SNL 2007, Appendix IV). The neptunium concentrations measured by Nitsche et al. (1993 and 1994) are plotted in Figure 1 for comparison purposes. At 90°C, Nitsche et al (1993) observed the formation of crystalline Np_2O_5 . In that case, as shown in Figure 1, the neptunium concentration observed is within two standard deviations of the model abstraction mean, and therefore falls within the range of uncertainty implemented in the neptunium abstraction (SNL 2007, Table 6.6-11).

Neck (2006, Figure 1) provides a plot of neptunium concentrations measured by several different sources for solutions in contact with $\text{NpO}_2\text{OH}(\text{am})$ in a carbonate-free system. At a pH of 8.5, Neck (2006, Figure 1) shows a neptunium concentration of approximately 150 mg/L. This solid is not an appropriate solubility-controlling phase because an amorphous solid, such as $\text{NpO}_2\text{OH}(\text{am})$, will age over time to a more crystalline, less soluble solid. In addition, the carbonate-free conditions of the experiments, which lead to lower neptunium concentrations when compared to carbonate systems, are not consistent with the repository atmosphere which is expected to have a CO_2 partial pressure of approximately 0.001 bars. For comparison with the other experimental values, the neptunium concentration from Neck (2006) is plotted in Figure 1.

In conclusion, none of the cited references provides concentration measurements that are inconsistent with the Np_2O_5 model abstraction used in the TSPA. In most cases, the data are not applicable due to the formation of metastable neptunium phases. In one case, the measured solubility value for the appropriate solid (Np_2O_5) is within two standard deviations of the model abstraction. All of the experimental values are plotted in Figure 1 for comparison with the model abstraction used in the TSPA.

Figure 1 Np₂O₅ Model Abstraction and Experimentally Observed Neptunium Concentrations

2. COMMITMENTS TO NRC

None.

3. DESCRIPTION OF PROPOSED LA CHANGE

None.

4. REFERENCES

Efurd, D.W.; Runde, W.; Banar, J.C.; Janecky, D.R.; Kaszuba, J.P.; Palmer, P.D.; Roensch, F.R.; and Tait, C.D. 1998. "Neptunium and Plutonium Solubilities in a Yucca Mountain Groundwater." *Environmental Science & Technology*, 32, (24), 3893-3900. Easton, Pennsylvania: American Chemical Society.

Neck, V. 2006. "Comment on Hydrolysis of Neptunium(V) at Variable Temperatures (10–85°C) by L. Rao, T.G. Srinivasan, A. Yu. Garnov, P. Zanonato, P. Di Bernardo, and A. Bismondo." *Geochimica et Cosmochimica Acta*, 70, 4551–4555.

Nitsche, H.; Gatti, R.C.; Standifer, E.M.; Lee, S.C.; Müller, A.; Prussin, T.; Deinhammer, R.S.; Maurer, H.; Bechart, K.; Leung, S.; and Carpenter, S.A. 1993. *Measured Solubilities and*

ENCLOSURE 12

Response Tracking Number: 00262-00-00

RAI: 3.2.2.1.3.4-013

Speciations of Neptunium, Plutonium, and Americium in a Typical Groundwater (J-13) from the Yucca Mountain Region. LA-12562-MS. Los Alamos, New Mexico: Los Alamos National Laboratory.

Nitsche, H.; Roberts, K.; Prussin, T.; Muller, A.; Becraft, K.; Keeney, D.; Carpenter, S.A.; and Gatti, R.C. 1994. *Measured Solubilities and Speciations from Oversaturation Experiments of Neptunium, Plutonium, and Americium in UE-25P #1 Well Water from the Yucca Mountain Region Milestone Report 3329-WBS1.2.3.4.1.3.1.* LA-12563-MS. Los Alamos, New Mexico: Los Alamos National Laboratory.

SNL (Sandia National Laboratories) 2007. *Dissolved Concentration Limits of Elements with Radioactive Isotopes.* ANL-WIS-MD-000010 REV 06. Las Vegas, Nevada: Sandia National Laboratory. ACC: DOC.20070918.0010.

RAI: Volume 3, Chapter 2.2.1.3.4, First Set, Number 14:

Provide the basis for confidence that the U and Np concentration limit abstractions are appropriate with respect to uncertainty in the dissolved Na concentration.

Basis: Over portions of the ranges of chemical conditions in their respective concentration limits abstractions, U will be controlled by the solubility of sodium boltwoodite ($\text{NaUO}_2\text{SiO}_3\text{OH} \cdot 1.5\text{H}_2\text{O}$) or $\text{Na}_4\text{UO}_2(\text{CO}_3)_3$, and Np by the solubility of $\text{NaNpO}_2\text{CO}_3$ (SAR Section 2.3.7.10.3). Under solubility control by these solids, the U or Np aqueous concentration will be directly related to the Na aqueous concentration by the solubility reaction equilibrium constant. The U and Np concentration limits and release rates, therefore, could strongly depend on the dissolved Na content in the waste form domain, corrosion products domain, and the invert. The requested information is needed to verify compliance with 10 CFR 63.21(c)(11)-(15) and 63.114(b).

1. RESPONSE

The effect of uncertainty in dissolved sodium on uranium and neptunium concentrations predicted by the dissolved concentrations model is minimal. Uranium and neptunium releases are controlled by solubility reactions involving, respectively, Na-boltwoodite and NpO_2 or Np_2O_5 . The effect of sodium concentrations on Na-boltwoodite solubilities and uranium release has been adequately accounted for. Neptunium release is not directly affected by sodium concentrations.

Sodium will be present in breached waste packages, waste form corrosion products, and the invert only if it is brought there by seepage from pore waters or basalts in the igneous scenario, or by dissolution of high-level waste (HLW) glass inside breached codisposal waste packages (some residual sodium from container cleaning might be present as well). In Yucca Mountain pore waters, Yucca Mountain well water (J-13), and basalt-contacted waters, Na^+ and Ca^{2+} are the most abundant cations. Sodium concentrations (and pH) will be high in breached codisposal waste packages because Na^+ leaches out of HLW glass, which is 11.4% to 12.3% Na_2O by weight.

1.1 SODIUM IN URANIUM SOLUBILITY CALCULATIONS

Fluid interaction inside breached waste packages is modeled as occurring in two cells: Cell 1 includes fuel elements and some metals; Cell 2 contains only corrosion products and steels. Codisposal fuel elements are further subdivided into Cell 1a, containing HLW glass, and Cell 1b, containing SNF (SAR Section 2.3.7.5.3). Because Na^+ is used as the default cation to maintain electrical balance in the solubility calculations described in the dissolved concentrations model (SNL 2007), there is the potential for Na^+ concentrations to be high, and possibly over-estimated, particularly at high pH in Cell 1a (maximum pHs of 7 to 10.5; SAR Figure 2.3.7-20) where substantial amounts of Na^+ are required to balance the OH^- , HCO_3^- , and CO_3^{2-} that automatically appear in the calculation. Comparison of SAR Figures 2.3.7-19, 2.3.7-20, 2.3.7-

21, and 2.3.7-31 shows that $\text{Na}_4\text{UO}_2(\text{CO}_3)_3$ is only stable in Cell 1a. Because Cell 1a fluids must move through Cell 1b before they can move into the corrosion product domain and then into the invert, uranium release is ultimately determined by Na-boltwoodite (and schoepite) solubility reactions occurring under the lower pH conditions of Cell 1b (maximum pHs of 7 to 9; SAR Figure 2.3.7-21). The Na^+ concentration needed to balance solution charge in the Cell 1b solubility calculation is much less than in the Cell 1a calculation because pHs are lower in Cell 1b than in Cell 1a. Fluids moving from Cell 1a into Cell 1b will possess initially high Na^+ concentrations from dissolving HLW glass (Na/U ratio = 56); conversion of schoepite (from MOX alteration) to Na-Boltwoodite will, however, consume some Na^+ . Na^+ inputs to Cell 1b will be high, consistent with Na^+ being used as the charge balancing cation in the Cell 1b solubility calculation.

Na-boltwoodite can also control uranium concentrations in the igneous scenario when seepage contacts commercial spent nuclear fuel (SNF) or DOE-owned SNF. Na^+ is specifically added to balance the charge in the solubility calculations only when pH is greater than near neutral. Because commercial SNF and DOE SNF cell pH values cannot be higher than 9 (SAR Figures 2.3.7-19 and 2.3.7-21), the pH range where Na^+ is used for charge balancing is relatively small. Na^+ is abundant in basalt-equilibrated waters, particularly high pH ones, consistent with Na^+ being the charge-balancing cation for pH 8 to 9 solutions.

The high concentrations of Na^+ in seepage and dissolving HLW glass make it unlikely that Na^+ concentrations have been overestimated in uranium and neptunium solubility calculations in the packages. Downstream Na^+ concentrations in the corrosion products and invert are appropriate as well because Na^+ will remain the dominant cation under the relatively restricted pH ranges of both domains.

Sodium concentration uncertainty, due primarily to sodium used in charge balance of water composition in modeling, has little effect on the solubility limit abstractions that are used to predict uranium concentrations

1.2 SODIUM IN NEPTUNIUM SOLUBILITY CALCULATIONS

$\text{NaNpO}_2\text{CO}_3$ is stable only at relatively high pH values (SNL 2007, Tables 6.6-2 and 6.6-8) that exist in Cell 1a of codisposal waste packages. As Cell 1a fluids must move through Cell 1b, neptunium release concentrations will be set not by $\text{NaNpO}_2\text{CO}_3$, which is unstable at the lower pHs of Cell 1b (7 to 9), but by NpO_2 or Np_2O_5 . This means that charge balancing with Na^+ has no impact on neptunium release concentrations.

Sodium concentration uncertainty, due primarily to sodium used in charge balance of water composition in modeling, has little effect on the solubility limit abstractions that are used to predict neptunium concentrations.

2. COMMITMENTS TO NRC

None.

3. DESCRIPTION OF PROPOSED LA CHANGE

None.

4. REFERENCES

SNL 2007. *Dissolved Concentration Limits of Elements with Radioactive Isotopes*. ANL-WIS-MD-000010 REV 06. Las Vegas, Nevada: Sandia National Laboratory.
ACC: DOC.20070918.0010.

RAI: Volume 3, Chapter 2.2.1.3.4, First Set, Number 15:

Development of the NpO_2 solubility model and the adjusted-Eh Pu model assumed the presence of carbon steel in the CSNF waste packages (Appendices IV and V of SNL, 2007a). Provide the technical bases to justify the use of these models given that carbon steel is no longer incorporated into the CSNF waste package design. Provide the technical basis in terms of (i) the quantitative/qualitative impact on these models and release rates and (ii) propagation of uncertainty from these models through the TSPA-LA.

Basis: The requested information is needed to verify compliance with 10 CFR 63.21(c)(3), (9), and (11)-(15) and 63.114(a), (b), and (g).

1. RESPONSE

The change in the design of commercial spent nuclear fuel (SNF) waste package materials to exclude carbon steel has no effect on the plutonium or neptunium solubility model outputs to the total system performance assessment (TSPA) for the license application (LA). There is no impact on release rates of plutonium and neptunium or propagation of uncertainty from the models through the TSPA as discussed below.

The adjusted-Eh model does not result in an underestimation of plutonium solubility even though carbon steel is no longer incorporated into the commercial SNF waste package design. As indicated in *Dissolved Concentration Limits of Elements with Radioactive Isotopes* (SNL 2007, Sections V.2 and V.5), the adjusted-Eh equation is developed by comparing results from the plutonium solubility model runs with experimental results on plutonium solubility and does not depend on the presence of carbon steel. However, it should be noted that the expected Eh of the water within the waste package will be dramatically influenced by the presence of steel (carbon or stainless) and SNF. The oxidation of SNF and steel will control the effective Eh of water within the waste package, keeping the system reducing, thus further lowering the solubility limits of plutonium below those presented for the adjusted-Eh.

The choice of neptunium solubility controlling phases is discussed in SAR Section 2.4.2.3.2.1.7 and in more detail in *Dissolved Concentration Limits of Elements with Radioactive Isotopes* (SNL 2007, Section 6.6 and Appendix IV). The NpO_2 solubility model is used within waste packages when reductants such as SNF and/or steel (carbon or stainless) remain. After reductants within waste packages are consumed, Np_2O_5 is assumed to be the solubility-controlling mineral phase. Therefore, the change in the commercial SNF waste package design has no impact on the neptunium model results presented in *Dissolved Concentration Limits of Elements with Radioactive Isotopes* (SNL 2007, Section 6.6) as there are still reducing materials (fuel and stainless steel) in the waste packages.

In summary, the change in the design of commercial SNF waste package materials to exclude carbon steel has no effect on the plutonium or neptunium solubility model outputs to the TSPA-LA. The adjusted-Eh model does not assume the presence of carbon steel or any other reductants but is developed by comparing results from plutonium solubility model runs with

experimental results of plutonium solubility. Additionally, the corrosion of stainless steel and SNF will ultimately lower redox conditions within the waste package. Thus, the adjusted-Eh model does not result in an underestimation of plutonium solubility if carbon steel is not incorporated into the commercial SNF waste package design. Furthermore, validity of the NpO_2 solubility model does not solely rely on the presence of carbon steel. The existence of other reductants, such as stainless steel and SNF, also makes it a valid model. Therefore, there is no impact on release rates of plutonium and neptunium or propagation of uncertainty from the models through the TSPA.

2. COMMITMENTS TO NRC

None.

3. DESCRIPTION OF PROPOSED LA CHANGE

None.

4. REFERENCES

SNL (Sandia National Laboratories) 2007. *Dissolved Concentration Limits of Elements with Radioactive Isotopes*. ANL-WIS-MD-000010 REV 06. Las Vegas, Nevada: Sandia National Laboratory. ACC: DOC.20070918.0010.

RAI: Volume 3, Chapter 2.2.1.3.4, First Set, Number 16:

Clarify which thermodynamic databases, or modifications of same, were used for solubility calculations for each radioelement. Provide justification that the multiple thermodynamic databases used in calculating radioelement solubility are appropriately applied in a way consistent with the potential repository conditions. Provide information on the internal consistency of each modification of the thermodynamic database.

Basis: SNL (2007b) describes the development of three DOE databases developed for use in supporting the license application: *data0.ymp.r2*, *data0.ymp.r4*, and *data0.ymp.r5*. Because development of these databases continued during preparation of analysis model reports supporting SAR Section 2.3.7, it is not always clear which database was used for calculations for a given element. In addition, mention is made in SNL (2007a) of modifications made to the databases for particular purposes. The use of multiple databases should be consistent with expected conditions and processes in the EBS. In addition, each database must maintain internal consistency among thermodynamic parameters. The requested information is needed to verify compliance with 10 CFR 63.21(c)(11)-(15) and 63.114(b).

1. RESPONSE

The *data0.ymp.R5* database was not used for solubility calculations in support of SAR Section 2.3.7. This response provides clarification regarding the use and application of the different versions of the thermodynamic databases *data0.ymp.R2* and *data0.ymp.R4* within *Dissolved Concentration Limits of Elements with Radioactive Isotopes* (SNL 2007a) and their consistency with calculations of solubility limits. Also provided is an explanation of how the effects of potential repository conditions on the solubilities of radioelements are addressed.

1.1 THERMODYNAMIC DATABASES AND CONSISTENCY

Solubility calculations of radioelements supporting SAR Section 2.3.7 are taken from *Dissolved Concentration Limits of Elements with Radioactive Isotopes* (SNL 2007a). The thermodynamic databases used in *Dissolved Concentration Limits of Elements with Radioactive Isotopes* (SNL 2007a) are *data0.ymp.R2* and *data0.ymp.R4*. Table 1 lists the thermodynamic database, and any modifications, used to calculate the solubility limits of each radioelement in *Dissolved Concentration Limits of Elements with Radioactive Isotopes* (SNL 2007a).

Table 1. Thermodynamic Database Used for Each Radioelement

| Radioelement | Thermodynamic Database Used to Calculate Solubility | Modifications of the Thermodynamic Database |
|-----------------------------------------------------|---------------------------------------------------------------------------------------------------------------------------------------------------------------------------------------------------|------------------------------------------------------------------------------------------------------------------------------------------------------------------------------------------------------------------------------------------------------------------------------------------------------------------------------------------------------------------------------------------|
| Pu | <i>data0.ymp.R2</i> | None |
| Np U Th Am Pa (by analog with Np) Ra | <i>data0.ymp.R2</i> modified to <i>data0.yc3.R1</i> | <ol style="list-style-type: none"> Incorporated the updated equilibrium constant for sodium boltwoodite ($\text{NaUO}_2\text{SiO}_3\text{OH} \cdot 1.5\text{H}_2\text{O}$) (SNL 2007a, Section 4.1) Correction to the log K value and formula of the phase $\text{PuO}_2(\text{OH})_2 \cdot \text{H}_2\text{O}$ (SNL 2007a, Section 6.5.1) |
| Sn | <i>data0.ymp.R4</i> modified to <i>data0.sn5</i> | Solubility data for $\text{SnO}_2(\text{am})$, $\text{Sn}(\text{OH})_5^-$, and $\text{Sn}(\text{OH})_6^{2-}$ were updated with more recent data on the thermodynamics of Sn(IV) species (SNL 2007a, Section 6.19.1). This update is consistent with <i>data0.ymp.R5</i> . |
| Tc C I Cs Sr Se Cl | No database required. Dissolved concentrations controlled by dissolution rate of waste forms rather than by solubility limits (SNL 2007a, Sections 6.14, 6.15, 6.16, 6.17, 6.18, 6.20, and 6.21). | |
| Ac Pb | No database required. TSPA assumes secular equilibrium with ^{231}Pa and ^{226}Ra , respectively (SNL 2007a, Sections 6.10 and 6.13). | |

Source: SNL 2007a.

The sources of thermodynamic data for the radioelements for *data0.ymp.R5*, and their associated phases, are documented in *Qualification of Thermodynamic Data for Geochemical Modeling of Mineral-Water Interactions in Dilute Systems* (SNL 2007b). The *data0.ymp.R2* and *data0.ymp.R4* thermodynamic databases share common origins for many of the chemical species presented in *data0.ymp.R5*. Specific updates to thermodynamic databases are shown in Table 2. Also, as shown in Table 2, changes in the databases include revisions/additions to: thorium(IV) aqueous and solid species, stoichiometry for the solid $\text{PuO}_2(\text{OH})_2 \cdot \text{H}_2\text{O}$, plutonium and neptunium log K temperature extrapolations for solids, tin aqueous and solid species, uranium minerals observed to form in drip tests on commercial spent nuclear fuel (SNF), and key thermodynamic properties of some phosphate chemical species. These affect the results presented in *Dissolved Concentration Limits of Elements with Radioactive Isotopes* (SNL 2007a) as follows:

- Changes to thorium(IV) aqueous and solid species do not impact the solubility model in *Dissolved Concentration Limits of Elements with Radioactive Isotopes* (SNL 2007a, Section 6.8) since the results from this model are conservative in the estimation of dissolved concentration limits for this radioelement. Moreover, validation of the thorium solubility model (SNL 2007a, Section 7.2.5) was based on comparisons with the same data sources adopted for the updates in *data0.ymp.R5*.

- The revised stoichiometry for the solid $\text{PuO}_2(\text{OH})_2 \cdot \text{H}_2\text{O}$ does not impact the plutonium solubility model since this phase is not used as a solubility-controlling solid (SNL 2007a, Section 6.5.3.1).
- Corrections to values of log K temperature extrapolations for plutonium and neptunium solids do not impact the solubility model results because these corrections only affect log K values for temperatures above 25°C. All plutonium and neptunium solubility calculations in support of SAR Section 2.3.7 are at 25°C (SNL 2007a, Sections 6.3.3.3 and 6.4.2.2).
- Changes to tin aqueous and solid species in *Dissolved Concentration Limits of Elements with Radioactive Isotopes* (SNL 2007a, Section 6.19.1) are consistent with those in *data0.ymp.R5*.
- The addition of uranium minerals observed to form in drip tests on commercial SNF has no impact to *Dissolved Concentration Limits of Elements with Radioactive Isotopes* (SNL 2007a) since these minerals are not used as solubility controlling phases.
- Revisions to phosphate species is described in *Qualification of Thermodynamic Data for Geochemical Modeling of Mineral-Water Interactions in Dilute Systems* (SNL 2007b). These updates have no impact on any results in *Dissolved Concentration Limits of Elements with Radioactive Isotopes* (SNL 2007a) since phosphate species were not used as controlling phases, and there are only two species that appear in the modeling runs ($\text{UO}_2\text{HPO}_4(\text{aq})$ and UO_2PO_4^-). These two species occur for only short ranges of pH and do not constitute large quantities of the aqueous complexes (less than 5% at maximum occurrence) (SNL 2007a, Section 1).

The thermodynamic database *data0.ymp.R5* was not used in *Dissolved Concentration Limits of Elements with Radioactive Isotopes* (SNL 2007a). However, there is no impact to the results given in that report (SNL 2007a).

Table 2. Generalized Description of Changes/Revisions in the Thermodynamic Databases *data0.ymp.R2* and *data0.ymp.R4* Reflected in *data0.ymp.R4* and *data0.ymp.R5*, Respectively

| Database Change from <i>data0.ymp.R2</i> to <i>data0.ymp.R4</i> | Database Change from <i>data0.ymp.R4</i> to <i>data0.ymp.R5</i> |
|---------------------------------------------------------------------------------------------------------------------------------------------|----------------------------------------------------------------------------------------------------------------------------------------------------------------------------------------------------------|
| Corrected log K values for certain zeolite phases (SNL 2007b, Section 6.3.2) | Additions of CaSeO ₄ ·2H ₂ O and CaSeO ₄ (aq) (SNL 2007b, Section 4.1.11) |
| Correction of stoichiometry for the Pu phase PuO ₂ (OH) ₂ ·H ₂ O (SNL 2007b, Section 6.3.4.5) ^a | Kogarkoite data (SNL 2007b, Section 4.1.12) |
| Correction to log K values for HF ₂ ⁻ dissociation (SNL 2007b, Section 6.4) | Additions of Sn solid and aqueous species: SnO ₂ (am), Sn(OH) ₄ (aq), Sn(OH) ₅ ⁻ , Sn(OH) ₆ ⁻ (SNL 2007b, Section 4.1.13) ^a |
| Log K values for neptunium and plutonium solids (SNL 2007b, Section 6.3.4.5) ^a | NiMoO ₄ data (SNL 2007b, Section 4.1.14) |
| — | Revision of Th(IV) aqueous and solid species data (SNL 2007b, Section 4.1.15) ^a |
| — | Revision/addition of NiCO ₃ aqueous and solid species (SNL 2007b, Section 4.1.16) |
| — | Revision/addition of phosphate chemical species including actinides (SNL 2007b, Section 4.1.17) ^a |
| — | Additions of magnesium silicates: palygorskite, sepiolite, and poorly crystalline antigorite (SNL 2007b, Section 4.1.18) |
| — | Revisions of data for uranium oxy-hydrates and silicates (SNL 2007b, Section 4.1.19) ^a |
| — | Revision/addition of miscellaneous chromium solid and aqueous species (SNL 2007b, Section 4.1.20) |

^a Although these changes were made, they do not affect solubility calculation results in support of SAR Section 2.3.7 (see text for further discussion).

1.2 THERMODYNAMIC DATABASES AND ENGINEERED BARRIER SYSTEM CONDITIONS

Calculations of radioelement solubility limits applied in a manner consistent with the potential repository conditions involve limitations in terms of the ionic strength of solution. The B-dot equation and associated parameters used in the calculations of activity coefficients of charged aqueous species in the *data0.ymp.R2*, *data0.ymp.R4*, and *data0.ymp.R5* databases is found valid up to ionic strengths of about one molal. Estimations of activity coefficients using the B-dot method may be extended to ionic strengths between 1 and 3 molal by adding an additional uncertainty term. This activity coefficient uncertainty is applied by augmenting the log K uncertainty (SNL 2007a, Section 6.3.3.4). For ionic strength values ranging from 1 to 3 molal, the values for the log K uncertainties are equal to $((\varepsilon_1)^2 + 0.3^2)^{1/2}$, where ε_1 is the log K uncertainty value for ionic strengths less than one molal given in Table 8-2 of *Dissolved Concentration Limits of Elements with Radioactive Isotopes* (SNL 2007a) for plutonium, neptunium, uranium, thorium, americium, and tin. The only exception to this rule is the use of the solid Na₄UO₂(CO₃)₃ in the uranium solubility model (see SNL 2007a, Section 6.7.5.2, for discussions on the use of this phase). For Na₄UO₂(CO₃)₃ as the solubility-controlling solid, the log K uncertainty value given in Table 8-2 of *Dissolved Concentration Limits of Elements with Radioactive Isotopes* (SNL 2007a) already accounts for the square root of the mean addition of

± 0.3 to the uncertainty term. There is no activity coefficient uncertainty applied to log K uncertainty at ionic strength values less than one molal.

1.3 CONCLUSIONS

The thermodynamic databases *data0.ymp.R2* and *data0.ymp.R4* used in *Dissolved Concentration Limits of Elements with Radioactive Isotopes* (SNL 2007a), which supports SAR Section 2.3.7, are appropriately applied to the calculation of radioelement solubilities consistent with potential repository conditions. Although there were some changes to these databases during the development of *data0.ymp.R5*, the results for the radioelement solubility models presented in *Dissolved Concentration Limits of Elements with Radioactive Isotopes* (SNL 2007a) were not affected by the revisions in the adopted databases in that report. For example, changes made to *data0.ymp.R4* for the phosphate system do not affect the results in *Dissolved Concentration Limits of Elements with Radioactive Isotopes* (SNL 2007a) because no phosphorus-bearing solids are used as solubility-controlling phases in the model and do not constitute significant quantities of the aqueous complexes. Also, differences in the updated thermodynamic parameters for thorium(IV) in *data0.ymp.R5* relative to those in *data0.ymp.R2* are not expected to impact the solubility model results since these are deemed conservative in the estimation of the dissolved concentration limits of this radioelement. Effects on solution chemistry due to an increase in ionic strength above one molal in response to potential repository conditions are captured in the form of augmented uncertainties in the solubility of the relevant solids.

2. COMMITMENTS TO NRC

None

3. DESCRIPTION OF PROPOSED LA CHANGE

None

4. REFERENCES

SNL (Sandia National Laboratories) 2007a. *Dissolved Concentration Limits of Elements with Radioactive Isotopes*. ANL-WIS-MD-000010 REV 06. Las Vegas, Nevada: Sandia National Laboratories. ACC: DOC.20070918.0010.

SNL 2007b. *Qualification of Thermodynamic Data for Geochemical Modeling of Mineral-Water Interactions in Dilute Systems*. ANL-WIS-GS-000003 REV 01. Las Vegas, Nevada: Sandia National Laboratories. ACC: DOC.20070619.0007.

RAI Volume 3, Chapter 2.2.1.3.4, First Set, Number 1:

Provide bases or justification for not considering colloid formation and consequent multiple-layer sorption or precipitation of actinides (e.g., Pu-239) on colloids resulting from the fast dissolution of commercial spent nuclear fuel (SNF).

Basis: The applicant presented the model for radionuclide release from the commercial SNF matrix in SAR section 2.3.7.7.3.2. The model determines the fractional dissolution rate of the SNF matrix as a function of the effective surface area of the SNF, temperature, carbonate concentration in solution, oxygen partial pressure, and solution pH. To determine these parameter values, the applicant used results from flow-through tests and dripping tests (BSC, 2004a). The upper end of the range of dissolution rates was derived from flow-through tests in carbonate solutions. This portion of the range appears to have contributed to fast dissolution times for SNF (120 to 2,100 years). While fast dissolution rates could seem to be risk-conservative, not all consequent processes resulting from these dissolution rates appear to have been evaluated in the SAR. These consequent processes could increase overall release rates from the repository.

Fast matrix dissolution might result in colloid formation (Ahn, 1996) and therefore multiple-layer sorption or precipitation of actinides on colloids (e.g., uranophane or zirconium oxide colloids) as well as on groundwater colloids. Iron oxide colloids could also form in the waste form domain from the corrosion of the steels used in the waste package internals and the transportation aging and disposal (TAD) canister. The applicant observed the colloid formation in solution and the precipitation of actinides on the surface of the SNF and test vessels in the tests of bare SNF at 25 and 85 °C in slow replenished J-13 well water (Wilson, 1990a, 1990b). Faster dissolutions at higher temperatures and in earlier test times resulted in more colloid formation and precipitation. The requested Information is needed to verify compliance with 10 CFR 63.21(c)(9), (12) and (15) and 63.114(b) and (g).

1. RESPONSE

1.1 SUPER SATURATION OCCURS MAINLY AT THE FUEL SURFACE

Corrosion of the commercial spent nuclear fuel (SNF) matrix leads to super saturation of plutonium in the solution contacting the fuel with respect to the precipitating plutonium phases, and the steady-state over saturation will depend on the fuel dissolution rate as described by Ahn (1996). However, there is evidence that this super saturation occurs mainly at the corroding fuel surface, especially after a corrosion product rind builds up on the surface. This evidence is threefold. First it is observed that plutonium accumulates in a narrow band within the corrosion product rind (e.g. Buck et al. 2004; Ebert et al. 2006, Section 2). Second, the normalized filterable plutonium fractional release rate (per day) is at least five orders of magnitude lower than the corrosion rate of the fuel as estimated by the normalized fractional release rate of

technetium. Third, observations that the plutonium colloid concentrations generally decrease over time as commercial SNF corrodes are consistent with the hypothesis that the condensation process, that might otherwise produce colloids in the bulk solution, occurs preferentially in the local environment within the corrosion product layers as they build up over time on the corroding commercial SNF surfaces. This evidence is the basis of the assertion that significant super saturation within the bulk solution is unlikely in the repository environment even under fast commercial SNF degradation conditions because, as described on SAR page 2.3.7-61, “the large abundance of other sorbing materials will prevent the radionuclides from becoming saturated and nucleating free-floating particles.”

1.2 EMPIRICAL IRREVERSIBLE COLLOID MODELS

1.2.1 The Irreversible Commercial SNF Colloid Model

The formation of true colloids (for example plutonium dioxide colloids), multiple-layer sorption, and precipitation onto colloids are included in the empirical model of irreversible attachment of actinides onto commercial SNF colloids that were based on SNF degradation experiments (SNL 2007, Section 6.3.2.4). The distribution of the concentration of plutonium (10^{-10} to 5×10^{-6} mol/L) on commercial SNF waste form colloids (ZrO_2 colloids) in the irreversible SNF colloids model was obtained from the Series III Wilson (1990) SNF dissolution experiments. These tests were conducted at 25°C and 85°C under semi-static conditions for up to 174 days. In the first days of the experiment, little corrosion product rind could have formed on the fuel surface to reduce the release of super saturated solutions into the bulk solution and reduce the processes of true colloid formation, multiple layer sorption, and precipitation of actinides onto colloids within the bulk solution. The range of the concentration of plutonium implemented in the irreversible SNF colloid model included the results from the faster dissolutions at higher temperatures and at earlier test times before a significant corrosion rind could form.

1.2.2 The Irreversible Iron Oxyhyroxide (FeO_x) Colloid Model

True colloids are included in the irreversible FeO_x colloid model. The irreversible FeO_x colloid model provides the rate of sorption of plutonium onto iron oxyhyroxide (FeO_x) colloids. This rate was based on eight experiments by Lu (SNL 2007, Table 6-18), four each for dissolved plutonium(V) and colloidal plutonium(IV), using J-13 well water and synthetic J-13 well water on colloids of hematite (Fe_2O_3) and goethite ($FeOOH$). The highest sorption rates were obtained in the Fe_2O_3 -Synthetic J-13 well water system with plutonium(V) and colloidal plutonium(IV). These rates were used to calculate an upper range of the forward rate constant, k , of $0.048\ m^3/(m^2\ yr)$, which was rounded up to $0.05\ m^3/(m^2\ yr)$. Because plutonium true colloids were included in the experiments used to derive the forward rate constant, the irreversible FeO_x colloid model includes the effects of true colloids.

1.2.3 Reversible Colloid Models

Including multiple layer sorption and precipitation onto reversible colloids would duplicate the processes already accounted for in the irreversible colloid formation models. The Wilson (1990) and Argonne tests were performed with J-13 well water, so groundwater colloids were present.

In addition, uranium mineral colloids formed in these tests. Therefore the processes of multiple layer sorption and precipitation onto these colloids were included in the measured colloidal plutonium concentration, and thus implicitly included in the empirically based irreversible waste form colloid model.

1.3 CONCLUSION

There is evidence that the processes of colloid formation and consequent multiple-layer sorption or precipitation of actinides (e.g., ^{239}Pu) on colloids resulting from the fast dissolution of commercial SNF, occur mainly within the corrosion product rind once it has formed. The escape of colloids from the rind, or formation of actinide-containing colloids outside the rind, has been included in the empirical models of irreversible attachment of plutonium and americium to colloids.

2. COMMITMENTS TO NRC

None.

3. DESCRIPTION OF PROPOSED LA CHANGE

None.

4. REFERENCES

Ahn, T 1996. "Long-term Kinetic Effects and Colloid Formation in the Dissolution of LWR Spent Fuels." NUREG-1564. Washington, D.C.: U.S. Nuclear Regulatory Commission.

Buck, Edgar C.; Finn, Patricia A.; and Bates, John K. *Micron, Volume 35*, Issue 4, June 2004, pp. 235-243 "Electron energy-loss spectroscopy of anomalous plutonium behavior in nuclear waste materials."

Ebert, W.L.; Fortner, J.A.; Guelis, A.V.; and Cunnane, J.C. 2006. *FY 2006 Annual Report for Waste Form Testing Activities*. ANL-06/49. Argonne, Illinois: Argonne National Laboratory. ACC: LLR.20070503.0001.

SNL (Sandia National Laboratories) 2007. *Waste Form and In-Drift Colloids-Associated Radionuclide Concentrations: Abstraction and Summary*. MDL-EBS-PA-000004 REV 03. Las Vegas, Nevada: Sandia National Laboratories. ACC: DOC.20071018.0019.

Wilson, C. N. 1990. "Results from NNWSI Series 3 Spent Fuel Dissolution Tests." PNL-7170. Richland, Washington: Pacific Northwest Laboratory.